

# An Information-Theoretic Characterization of MIMO-FAS: Optimization, Diversity- Multiplexing Tradeoff and $q$ -Outage Capacity

Wee Kiat New, *Member, IEEE*, Kai-Kit Wong, *Fellow, IEEE*,

Hao Xu, *Member, IEEE*, Kin-Fai Tong, *Fellow, IEEE*, and

Chan-Byoung Chae, *Fellow, IEEE*

## Abstract

Multiple-input multiple-output (MIMO) system has been the defining mobile communications technology in recent generations. With the ever-increasing demands looming towards the sixth generation (6G), we are in need of additional degrees of freedom that deliver further gains beyond MIMO. To this goal, fluid antenna system (FAS) has emerged as a new way to obtain spatial diversity using reconfigurable position-switchable antennas. Considering the case with more than one ports activated on a 2D fluid antenna surface at both ends, we take the information-theoretic approach to study the achievable performance limits of the MIMO-FAS. First of all, we propose a suboptimal scheme, referred to as QR MIMO-FAS, to maximize the rate at high signal-to-noise ratio (SNR) via joint port selection, transmit and receive beamforming and power allocation. We then derive the optimal diversity and multiplexing tradeoff (DMT) of MIMO-FAS. From the DMT, we highlight that MIMO-FAS outperforms traditional MIMO antenna systems. Further, we introduce a new metric, namely  $q$ -outage capacity, which can jointly consider rate and outage probability. Through this metric, our results indicate that MIMO-FAS surpasses traditional MIMO greatly.

The work of W. K. New, K. K. Wong and K. F. Tong is supported by the Engineering and Physical Sciences Research Council (EPSRC) under grant EP/W026813/1. The work of C.-B. Chae is supported by the Institute for Information and Communication Technology Promotion (IITP) grant funded by the Ministry of Science and ICT (MSIT), Korea (No. 2021-0-02208, No. 2021-0-00486). The work of H. Xu is supported by the European Union's Horizon 2020 Research and Innovation Programme under Marie Skłodowska-Curie Grant No. 101024636.

W. K. New (email: a.new@ucl.ac.uk), K. K. Wong (corresponding author, email: kai-kit.wong@ucl.ac.uk), H. Xu (email: hao.xu@ucl.ac.uk), and K. F. Tong (email: k.tong@ucl.ac.uk) are with the Department of Electronic and Electrical Engineering, University College London, London, WC1E 6BT, United Kingdom. C.-B. Chae (email: cbchae@yonsei.ac.kr) is with the School of Integrated Technology, Yonsei University, Seoul 03722 Korea. K. K. Wong is also affiliated with Yonsei Frontier Lab., Yonsei University, Seoul 03722, Korea.

## Index Terms

6G, Diversity and multiplexing tradeoff, Fluid antenna system, MIMO, Outage capacity.

### I. INTRODUCTION

#### *A. Background*

Sixth-generation (6G) mobile communication seeks to push the key performance indicators (KPIs) way beyond what the current fifth generation (5G) promises to offer. Such upgrade will require new technologies that can achieve more from the same amount of bandwidth. Presently, the dominating technology has been multiple-input multiple-output (MIMO), which also comes in the form of multiuser MIMO and massive MIMO. In 6G, the desire is to exceed MIMO [1], [2].

To achieve this very ambitious goal, one emerging idea is fluid antenna system (FAS) [3]. FAS represents any software-controllable fluidic, conductive or dielectric structure that can adjust its shape and position to reconfigure the gain, radiation pattern, operating frequency and other radiation characteristics. This is now feasible, thanks to the recent advances in utilizing flexible conductive materials such as liquid metals or ionized solutions [4], switchable pixels [5], [6] and stepper motors for antennas [7], [8]. Unlike traditional antenna that is placed at a fixed location, fluid antenna is able to switch its location almost instantly in a limited space. The most basic single fluid antenna consists of one radio frequency (RF)-chain and  $N$  preset locations (also known as ports) that are distributed in a given space [3]. The radiating element of the fluid antenna can switch its position among these ports to obtain a higher rate, lower outage probability, lower interference and other desirable performance. As the ports can be placed closely to each other, the channels of these ports are strongly correlated and thus spatial correlation plays a crucial role in FAS.

The main implementation designs for FAS are: i) liquid-based fluid antenna and ii) RF pixel-based fluid antenna. In the liquid-based fluid antenna, each liquid droplet can precisely switch its position by controlling the electric field using the thin conductive lines on top of the dielectric layer while other technology may use an electronically controlled pump to shift the position of a fluid radiating element in a tube. On the other hand, in the RF pixel-based fluid antenna, the RF pixels can be turned on-and-off instantly regardless of the surface area. One or several pixels when on, form an antenna port for transmission or reception like a standard antenna. Besides,

each activated port is connected to an RF-chain, operating like a conventional antenna. In short, the basic principle of FAS is to exploit the dynamic nature of fluid antenna to achieve ultimate flexibility for diversity and multiplexing gains.<sup>1</sup>

Due to its unprecedented benefits, single-user, single-input single-output (SISO)-FAS has recently been investigated under different scenarios and assumptions. Specifically, as the number of ports increases, [9] showed that the outage probability of FAS could be reduced drastically while [10] demonstrated that FAS could significantly improve the ergodic capacity. Motivated by these works, [11] derived the level crossing rate, [12] devised a port selection algorithm by observing the channels of a few ports, [13] investigated the performance of FAS over general correlated channels and [14] analyzed the outage probability of FAS for Terahertz communications while selection combining and maximum gain combining were further considered. Optimistic results were obtained in these works but it was illustrated in [15] that the outage probability of FAS could only be reduced to a floor when a more accurate spatial correlation model was adopted. The recent work [16] explained such limitations at an intuitive level and revealed that the performance of FAS was generally determined by the available space. Moreover, only in certain cases might FAS achieve a similar outage probability as compared to the classical maximal ratio combining (MRC) system.

The unique ability of switching the antenna position finely in FAS can also be exploited to mitigate interference, which would be impractical in traditional antenna selection systems. Recently, [17] investigated orthogonal multiple access to serve multiple users with fluid antennas while [18] used a space division multiple access approach to minimize the user transmit power. Nevertheless, an arguably more interesting idea is the fluid antenna multiple access (FAMA) scheme [19] where the rationale is to exploit the moment of deep fades in the spatial domain to alleviate inter-user interference. FAMA is classified into slow FAMA and fast FAMA in which the earlier switches its port when the channel changes [20] and the latter switches its port on a symbol-by-symbol basis [21]. Most recently, the outage probability for two-user FAMA was studied in [22].

In summary, FAS has shown promises but much is still not well understood. For example, the performance of FAS itself can be lifted if more than one ports are activated. For a point-to-point

<sup>1</sup>It is worth pointing out that FAS does not necessarily use ‘fluid’ materials for antenna and in wireless communications that requires adaptation in time of milliseconds or less, reconfigurable pixels are more relevant.

communication channel, we refer to the system where both ends are equipped with a multi-port FAS, as MIMO-FAS which is also known as fluid MIMO or flexible MIMO in [3]. Compared to a traditional MIMO antenna selection system in which the number of antennas is limited in a given surface (at least half wavelength separation between the antennas) and the antennas are fixed in positions, MIMO-FAS is distinct in the sense that the positions of the radiating elements can be dynamically and finely adjusted and that the number of preset locations (i.e., ports) within a given surface can be arbitrarily large, which yields additional gains. Note that FAS has also been proposed for multiple access recently [20]–[22], where the fine resolution of FAS is absolutely essential and conventional antenna selection would be unable to cope.

It is anticipated that the capacity and reliability of MIMO-FAS will be improved over the SISO counterpart. In fact, a related work showed that the capacity of a movable antenna system (which can be interpreted as a specific version of MIMO-FAS) could be improved up to 42% as compared to traditional MIMO systems [23]. In the study, however, spatial correlation between the antenna positions was not considered. Plus, more importantly, the optimal diversity and multiplexing tradeoff (DMT) of MIMO-FAS is still unknown.

In information theory, the optimal DMT can be employed as a unified framework to compare the performance of different multiple-antenna systems [24]. More concretely, it focuses on the asymptotic high signal-to-noise ratio (SNR) regime and a scheme is then said to achieve a multiplexing gain of  $r$  and a diversity gain of  $d(r)$  if the rate of the system scales like  $r \log \text{SNR}$  and its outage probability decays like  $\text{SNR}^{-d(r)}$ . It is known that  $r$  cannot exceed the total degrees of freedom of the channel and  $d(0)$  is limited by the maximal diversity gain, i.e., total number of independent channels. In between the two extremes, a system must tradeoff each type of gains.

## B. Contributions

Motivated by this, this paper analyzes the performance of MIMO-FAS with the goal of gaining useful insights for designing an efficient MIMO-FAS. To this end, we first develop a system model of MIMO-FAS while taking into account of the spatial correlation effect. We then propose a suboptimal scheme that maximizes the rate of MIMO-FAS through joint port selection, transmit and receive beamforming and power allocation at high SNR. Based on this scheme, we derive the optimal DMT of MIMO-FAS to reveal the fundamental limits of MIMO-FAS from an information-theoretic viewpoint. From the analytical results, we further study the effects of different MIMO-FAS parameters and reveal the superiority of MIMO-FAS over traditional

MIMO and MIMO antenna selection in terms of DMT. In addition, we introduce a new metric, referred to as  $q$ -outage capacity, to showcase the benefits of MIMO-FAS. Our main contributions are summarized as follows:

- We develop a system model for MIMO-FAS with a two-dimensional (2D) fluid antenna surface at both ends while taking into account of the spatial correlation of the ports. In particular, we employ a simple yet accurate channel model that considers the spatial correlation in a three-dimensional (3D) scattering environment. Based on this channel model, we introduce several system parameters such as active ports, beamforming matrices and power allocation. The achievable rate of MIMO-FAS is then derived where its expression resembles the rate of a traditional MIMO system.
- Also, we formulate a non-convex optimization problem to maximize the rate of MIMO-FAS via joint port selection, transmit and receive beamforming and power allocation. We show that the global optimal solution can be obtained using an exhaustive search, singular value decomposition (SVD) and waterfilling power allocation, at the expense of a non-polynomial time complexity. To reduce the time complexity, we propose the QR MIMO-FAS scheme that maximizes the rate of MIMO-FAS at high SNR via suboptimal port selection, beamforming and power allocation. It is shown that QR MIMO-FAS has a polynomial time complexity.
- Furthermore, we derive the outer bound of the DMT of MIMO-FAS. By using the outer bound and QR MIMO-FAS, we obtain the optimal DMT of MIMO-FAS. In this process, we prove that the spatial correlation matrix  $\mathbf{J}_s$  can be represented by a finite-size matrix  $\mathbf{J}_{\text{red}}^s$  even if the number of ports increases to infinity. Afterwards, we propose methods to estimate the size of  $\mathbf{J}_{\text{red}}^s$  and linearly transform between  $\mathbf{J}_s$  and  $\mathbf{J}_{\text{red}}^s$  with proof of certificates.
- Extensive results are provided to highlight the effects of several MIMO-FAS parameters. In the discussions, we provide useful insights for designing an efficient MIMO-FAS. Although MIMO-FAS provides rate improvements over the traditional MIMO antenna systems, we highlight that the superiority of MIMO-FAS actually lies in the diversity gain. Specifically, the diversity gain of MIMO-FAS for a fixed  $r$  is much greater than that of MIMO and MIMO antenna selection if the total number of active ports or antennas is the same.
- Finally, we introduce a new performance metric, referred to as  $q$ -outage capacity, that jointly considers both rate and outage probability. We show that MIMO-FAS outperforms

the traditional MIMO and MIMO antenna selection in terms of  $q$ -outage capacity. This result suggests that MIMO-FAS is more reliable in delivering high data rate transmission than the traditional MIMO systems.

### C. Organization and Notations

The remainder of this paper is organized as follows. Section II introduces the system model of MIMO-FAS. Section III details the proposed QR MIMO-FAS scheme that maximizes its rate at high SNR. The optimal DMT of MIMO-FAS is analyzed in Section IV. Section V presents the numerical results to compare MIMO-FAS with the traditional MIMO systems and we conclude the paper in Section VI.

Throughout this paper, scalar variables are denoted by italic letters (e.g.,  $c$ ), vectors are denoted by boldface italic small letters (e.g.,  $\mathbf{c}$ ) and matrices are denoted by boldface italic capital letters (e.g.,  $\mathbf{C}$ ). Additionally,  $(\cdot)^T$  denotes transpose,  $(\cdot)^H$  denotes conjugate transpose while  $\det(\cdot)$ ,  $\text{rank}(\cdot)$  and  $\text{trace}(\cdot)$  represent the determinant, rank and trace of a matrix, respectively. Moreover,  $|\cdot|$ ,  $\|\cdot\|_2$  and  $\|\cdot\|_F$  denote the absolute, Euclidean norm and Frobenius norm operations, respectively. Furthermore, we use  $\log(\cdot)$  to denote logarithm with base 2,  $[\cdot]_c^+$  outputs the argument that is lower bounded by  $c$ ,  $\min\{\cdot\}$  and  $\max\{\cdot\}$  denote the minimum and maximum value of the argument, respectively.  $\mathbb{E}[\cdot]$  returns the expected value of the input random quantity, and  $\otimes$  denotes the Kronecker product. Finally,  $\mathbf{e}_k$  represents an all-zero vector except the  $k$ -th entry being unity,  $\text{diag}(\cdot)$  denotes a diagonal matrix whose diagonal entries are the inputs, and  $(\cdot)^\dagger$  denotes the pseudoinverse of an input matrix. To help readers follow the mathematical contents, the meanings of the key variables are listed in Table I.

## II. SYSTEM MODEL

As illustrated in Fig. 1, we consider a point-to-point wireless communication channel in which the transmitter and receiver are equipped with a fluid antenna. To facilitate our discussions, we use the subscript/superscript  $s$  to denote the parameters at the transmitter or receiver as  $tx$  or  $rx$ , respectively, i.e.,  $s \in \{tx, rx\}$ . We assume that the fluid antenna takes up a 2D space with an area of  $W_s$  and has  $N_s$  ports spread uniformly over the 2D space. A grid structure is considered where  $N_i^s$  ports are uniformly distributed along a linear space of length  $\lambda W_i^s$  for  $i \in \{1, 2\}$ , so that  $N_s = N_1^s \times N_2^s$  and  $W_s = W_1^s \times W_2^s$ , where  $\lambda$  is the wavelength of the carrier frequency.

Table I: The meanings of the key notations

Notation	Meaning
$\mathbf{A}$	Activation port matrices at both of the transmitter and receiver sides
$\mathbf{A}_s$	Activation port matrix at side $s$
$C_{\text{sys}}^q$	$q$ -outage capacity of a system
$d(r)$	Diversity gain for $r$ multiplexing gain
$\mathbf{G}$	Circularly symmetric complex Gaussian matrix with i.i.d. entries
$\mathbf{H}$	Complex channels of MIMO-FAS
$\bar{\mathbf{H}}$	Complex channels of the activated ports
$\mathbf{H}_a$	Partial channels of the active ports
$\mathbf{H}_i$	Partial channels of the inactive ports
$\mathbf{J}_s$	Spatial correlation matrix at side $s$
$\hat{\mathbf{J}}_s$	Approximated matrix of $\mathbf{J}_s$
$\mathbf{J}_{\text{red}}^s$	Full rank spatial correlation matrix at side $s$
$\mathbf{K}$	Input covariance
$n_s$	Total number of active ports
$n_{\text{max}}/n_{\text{min}}$	Maximum/minimum of $n_{rx}$ and $n_{tx}$
$N_{\text{max}}/N_{\text{min}}$	Maximum/minimum of $N_{rx}$ and $N_{tx}$
$N_s$	Total number of ports at side $s$
$N_i^s$	Number of ports in the $i$ -th dimension at side $s$
$N'_s$	Rank of $\mathbf{J}_{\text{red}}^s$
$N'_{\text{min}}$	Minimum of $N'_{rx}$ and $N'_{tx}$
$P_{\text{sys}}^{\text{out}}(\text{SNR}, r)$	Outage probability of a system in terms of $r$ log SNR
$\bar{P}_{\text{sys}}^{\text{out}}(\text{SNR}, q)$	Outage probability of a system for a fixed $q$ -transmission rate
$\mathbf{P}$	Power allocation matrix
$r$	Multiplexing gain
$R_{\text{sys}}(\text{SNR})$	Rate of a system for a given SNR
$s \in \{tx, rx\}$	Subscript/superscript to denote the transmit/receiver side
SNR	Transmit SNR
$\mathbf{v}_l^s$	Certificate between the linear transformation of $\mathbf{J}_s^{(l)}$ and $\mathbf{J}_{\text{sub}}^{(l-1)}$
$W_s$	Total area of the fluid antenna at side $s$
$W_i^s$	Length of the fluid antenna in the $i$ -th dimension at side $s$
$\mathbf{W}$	Transmit and receive beamforming matrices
$\mathbf{W}_s$	Beamforming matrix at $s$ side
$\lambda$	Wavelength of the carrier frequency
$\Lambda_s$	Matrix whose diagonal entries are the eigenvalues of $\mathbf{J}_s$
$\Sigma$	Matrix whose diagonal entries are singular values of $\mathbf{H}$
$\bar{\Sigma}$	Matrix whose diagonal entries are singular values of $\bar{\mathbf{H}}$
$\Omega$	Special matrix used for port optimization

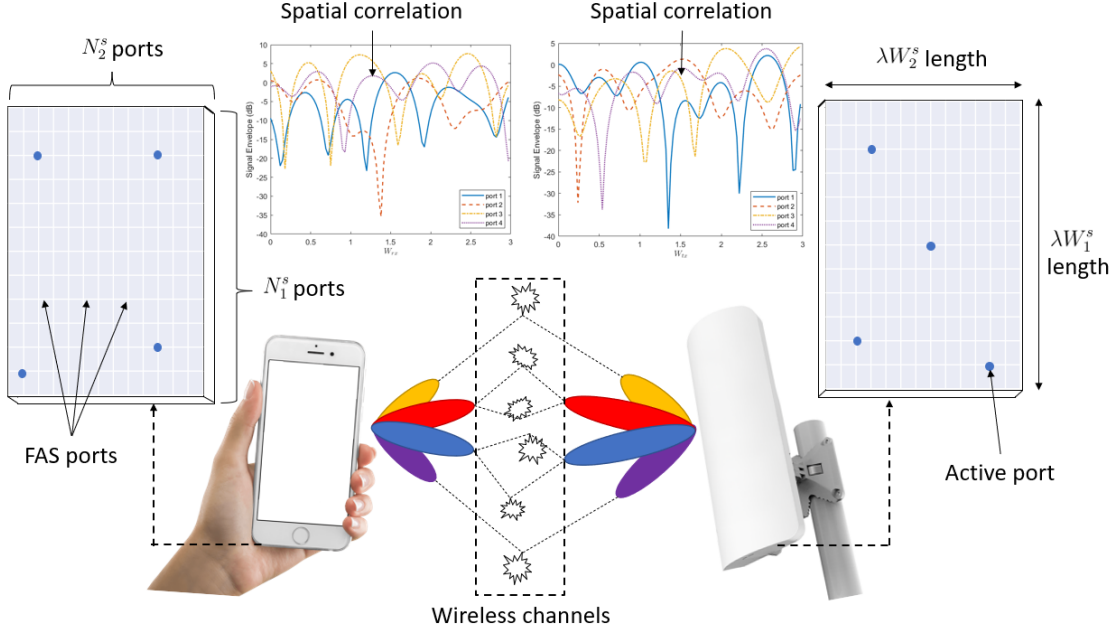


Figure 1: A schematic of point-to-point MIMO-FAS.

In this MIMO-FAS, the transmitter and receiver can only activate  $n_s$  out of  $N_s$  ports. Note that for SISO-FAS,  $n_s = 1, \forall s$ .

Considering a 3D scattering environment under rich scattering, the spatial correlation between the  $(n_1^s, n_2^s)$ -th port and the  $(\tilde{n}_1^s, \tilde{n}_2^s)$ -th port is given by

$$J_{(n_1^s, n_2^s), (\tilde{n}_1^s, \tilde{n}_2^s)}^s = \delta_s^2 j_0 \left( 2\pi \sqrt{\left( \frac{|n_1^s - \tilde{n}_1^s|}{N_1^s - 1} W_1^s \right)^2 + \left( \frac{|n_2^s - \tilde{n}_2^s|}{N_2^s - 1} W_2^s \right)^2} \right), \quad (1)$$

where  $j_0(\cdot)$  is the spherical Bessel function of the first kind,  $\delta_{rx}^2$  can be used to account for the large-scale fading effect and  $\delta_{tx}^2 = 1$ .<sup>2</sup> A detailed proof can be found in Appendix I. As seen in (1), it is cumbersome to label a port in 2D. To simplify our notations, we use the function  $\text{map} : \mathbb{R}^2 \rightarrow \mathbb{R}$ , e.g.,  $\text{map}(n_1^s, n_2^s) = l_s$ , where  $l_s \in \{1, \dots, N_s\}$ .

<sup>2</sup>Note that (1) can be reduced to a 1D fluid antenna under 2D scattering environments by setting  $N_2^s = 1$  and  $\frac{0}{0} \triangleq 0$  and replacing  $j_0(\cdot)$  by  $J_0(\cdot)$  where  $J_0(\cdot)$  is the Bessel function of the first kind. Furthermore,  $\delta_{tx}^2$  is mainly introduced for consistency.



Using the mapping function, we can express the spatial correlation matrix  $\mathbf{J}_s$  as

$$\mathbf{J}_s = \begin{bmatrix} J_{1,1}^s & J_{1,2}^s & \cdots & J_{1,N_s}^s \\ J_{2,1}^s & J_{2,2}^s & \cdots & J_{2,N_s}^s \\ \vdots & \vdots & \ddots & \vdots \\ J_{N_s,1}^s & J_{N_s,2}^s & \cdots & J_{N_s,N_s}^s \end{bmatrix}, \quad (2)$$

where  $J_{k_s,l_s}^s$  is the spatial correlation of the  $k_s$ -th and the  $l_s$ -th port at side  $s$ , and  $k_s$  and  $l_s$  are the labels after mapping. Since  $J_{k_s,l_s}^s = J_{l_s,k_s}^s$ , (2) can be decomposed into  $\mathbf{J}_s = \mathbf{U}_s \mathbf{\Lambda}_s \mathbf{U}_s^H$  where  $\mathbf{U}_s$  is an  $N_s \times N_s$  matrix whose  $l$ -th column (i.e.,  $\mathbf{u}_l^s$ ) is the eigenvector of  $\mathbf{J}_s$  and  $\mathbf{\Lambda}_s = \text{diag}(\lambda_1^s, \dots, \lambda_{N_s}^s)$  is an  $N_s \times N_s$  diagonal matrix whose  $l$ -th diagonal entries are the corresponding eigenvalues of  $\mathbf{u}_l^s$ . Without loss of generality, we assume that the values of the eigenvalues in  $\mathbf{\Lambda}_s$  are in descending order, i.e.,  $\lambda_1^s \geq \dots \geq \lambda_{N_s}^s$ . Note that  $\mathbf{U}_s \mathbf{\Lambda}_s \mathbf{U}_s^H$  is computed independently for each  $s \in \{tx, rx\}$ .

Given  $\mathbf{U}_s$  and  $\mathbf{\Lambda}_s$  for  $\forall s$ , the complex channel of MIMO-FAS can be modelled as

$$\mathbf{H} = \mathbf{U}_{rx} \sqrt{\mathbf{\Lambda}_{rx}} \mathbf{G} \sqrt{\mathbf{\Lambda}_{tx}^H} \mathbf{U}_{tx}^H, \quad (3)$$

where  $\mathbf{G} = [\mathbf{g}_1, \dots, \mathbf{g}_{N_{tx}}]$ ,  $\mathbf{g}_l = [g_{1,l}, \dots, g_{N_{rx},l}]^T$ ,  $g_{k,l} = x_{k,l} + jy_{k,l}$ , and  $x_{k,l}, y_{k,l}$  are independent Gaussian random variables with zero mean and variance of  $\frac{1}{2}$ ,  $\forall k, l$ . Letting  $\mathbf{h}_{\text{vec}} = \text{vec}(\mathbf{H})$ , the covariance of  $\mathbf{h}_{\text{vec}}$  is  $\mathbf{J}_{tx}^T \otimes \mathbf{J}_{rx}$ . Thus, the channels of the  $k_s$ -th and  $l_s$ -th ports are precisely correlated according to (1).<sup>3</sup>

Next, we denote the activation port matrices at the transmitter and receiver, respectively, as  $\mathbf{A}_{tx} = [\mathbf{a}_1^{tx}, \dots, \mathbf{a}_{n_{tx}}^{tx}]$  and  $\mathbf{A}_{rx} = [\mathbf{a}_1^{rx}, \dots, \mathbf{a}_{n_{rx}}^{rx}]^T$ , where  $\mathbf{a}_l^{tx}$  and  $\mathbf{a}_l^{rx}$  are standard basis vector (i.e.,  $\mathbf{a}_l^s \in \{\mathbf{e}_1, \dots, \mathbf{e}_{N_s}\}$ ). Since only distinct  $n_s$  ports can be activated at a time, we have  $\mathbf{a}_k^{tx} \neq \mathbf{a}_l^{tx}$  and  $\mathbf{a}_k^{rx} \neq \mathbf{a}_l^{rx}$  if  $k \neq l$ . Let us further denote  $\mathbf{W}_{tx}$  and  $\mathbf{W}_{rx}$  as the transmit and receive beamforming matrices, with the constraint  $\|\mathbf{W}_s\|_2 = 1$ . Then the receive signal of MIMO-FAS can be rewritten as

$$\mathbf{W}_{rx} \mathbf{A}_{rx} \mathbf{Y} = \mathbf{W}_{rx} \mathbf{A}_{rx} \mathbf{H} \mathbf{A}_{tx} \mathbf{W}_{tx} \mathbf{x} + \mathbf{W}_{rx} \mathbf{A}_{rx} \mathbf{w} \quad (4)$$

$$\Rightarrow \tilde{\mathbf{Y}} = \tilde{\mathbf{H}} \mathbf{x} + \tilde{\mathbf{w}}, \quad (5)$$

<sup>3</sup>Due to the port spatial correlation, it can be shown that only a small number of observed ports/training is required to obtain the full channel state information regardless of the number of ports of the FAS [25]. Machine learning techniques have also been proposed to address the channel estimation problem for port selection in FAS, e.g., [20].

where  $\mathbf{x}$  is the information signal and  $\mathbf{w}$  is the additive white Gaussian noise with zero mean and identity covariance. In (5), we defined  $\tilde{\mathbf{Y}} \triangleq \mathbf{W}_{rx} \mathbf{A}_{rx} \mathbf{Y}$ ,  $\tilde{\mathbf{H}} \triangleq \mathbf{W}_{rx} \mathbf{A}_{rx} \mathbf{H} \mathbf{A}_{tx} \mathbf{W}_{tx}$  and  $\tilde{\mathbf{w}} \triangleq \mathbf{W}_{rx} \mathbf{A}_{rx} \mathbf{w}$ . For ease of expositions, we denote  $\mathbf{A} = [\mathbf{A}_{tx}, \mathbf{A}_{rx}]$ ,  $\mathbf{W} = [\mathbf{W}_{tx}, \mathbf{W}_{rx}]$ ,  $\bar{\mathbf{H}} = \mathbf{A}_{rx} \mathbf{H} \mathbf{A}_{tx}$  and  $\mathbf{K} = \mathbf{W}_{tx} \mathbf{P} \mathbf{W}_{tx}^H$  where  $\mathbf{K}$  is the input covariance and  $\mathbf{P} = \mathbb{E}[\mathbf{x} \mathbf{x}^H]$  is the power allocation matrix. Then, the rate of MIMO-FAS is given by

$$R(\mathbf{A}, \mathbf{W}, \mathbf{P}) = \log \det \left( \mathbf{I} + \bar{\mathbf{H}} \mathbf{K} \bar{\mathbf{H}}^H \right), \quad (6)$$

where  $\text{trace}(\mathbf{K}) \leq \text{SNR}$  and SNR is the transmit SNR.

### III. QR MIMO-FAS: SUBOPTIMAL PORT SELECTION, BEAMFORMING AND POWER ALLOCATION

In this section, we aim to maximize the rate of the MIMO-FAS via joint optimal port selection, beamforming and power allocation. The optimization problem is formulated as

$$\max_{\mathbf{A}, \mathbf{W}, \mathbf{P}} R(\mathbf{A}, \mathbf{W}, \mathbf{P}) \quad (7a)$$

$$\text{s.t. } \mathbf{a}_l^s \in \{e_1, \dots, e_{N_s}\}, s \in \{rx, tx\}, \forall l, \quad (7b)$$

$$\mathbf{a}_k^{tx} \neq \mathbf{a}_l^{tx}, \text{ if } k \neq l \quad (7c)$$

$$\mathbf{a}_k^{rx} \neq \mathbf{a}_l^{rx}, \text{ if } k \neq l \quad (7d)$$

$$\|\mathbf{W}_{tx}\|_2 = \|\mathbf{W}_{rx}\|_2 = 1 \quad (7e)$$

$$\text{trace}(\mathbf{K}) \leq \text{SNR}. \quad (7f)$$

Note that (7) is a non-convex optimization problem because i) the optimization variables are mutually coupled and ii) its domain is non-convex. A systematic way to solve this problem is to employ an exhaustive search [26], SVD and waterfilling power allocation [27]. In particular, the maximum rate of MIMO-FAS can be computed via SVD and waterfilling power allocation over  $\binom{N_{tx}}{n_{tx}} \times \binom{N_{rx}}{n_{rx}}$  port combinations.<sup>4</sup> Nevertheless, such a method requires a non-polynomial time complexity of  $\mathcal{O}(N_{tx}^{n_{tx}} N_{rx}^{n_{rx}})$  which is prohibitively high.

To reduce the time complexity, we propose a suboptimal scheme, namely QR MIMO-FAS, to maximize the rate of MIMO-FAS in the high SNR regime. This scheme is useful for analyzing the DMT of MIMO-FAS. In the proposed scheme, we decouple (7) into two subproblems:

<sup>4</sup>As shown later in this paper,  $N_s, \forall s$  can be represented by a finite constant even in cases where  $N_s \rightarrow \infty$ .

i) optimal port selection and ii) optimal beamforming and power allocation. For optimal port selection, (7) can be simplified as

$$\max_{\mathbf{A}} R(\mathbf{A}, \mathbf{W}, \mathbf{P}) \quad \text{s.t.} \quad (7b), (7c), (7d). \quad (8)$$

However, it is still challenging to solve (8) since the objective function cannot be directly evaluated. To overcome this problem, we exploit the fact that  $R(\mathbf{A}, \mathbf{W}, \mathbf{P})$  strongly depends on  $\det(\bar{\mathbf{H}}\bar{\mathbf{H}}^H)$  in the high SNR regime [28]. Thus, (8) can be relaxed as

$$\max_{\mathbf{A}} \det(\bar{\mathbf{H}}\bar{\mathbf{H}}^H) \quad \text{s.t.} \quad (7b), (7c), (7d), \quad (9)$$

which is unfortunately still an NP-hard problem [29].<sup>5</sup> However, we can obtain a suboptimal solution by using the strong rank-revealing QR (RRQR) factorization [30].

Specifically, by applying QR factorization with pivoted column on  $\mathbf{H}^H$ , we have

$$\mathbf{H}^H \mathbf{\Pi} = \mathbf{Q}\mathbf{R}, \quad (10)$$

where  $\mathbf{\Pi}$  is a permutation matrix,  $\mathbf{Q}$  is an orthogonal matrix and  $\mathbf{R}$  is an upper triangular matrix where the absolute of leading entries in  $\mathbf{R}$  are decreasing in values. The upper triangular matrix  $\mathbf{R}$  can be rewritten as

$$\mathbf{R} = [\mathbf{R}_1 \ \mathbf{R}_2] = \begin{bmatrix} \mathbf{S}_1 & \mathbf{S}_2 \\ \mathbf{0} & \mathbf{S}_3 \end{bmatrix}, \quad (11)$$

where  $\mathbf{R}_1 = [\mathbf{S}_1 \ \mathbf{0}]^T$  and  $\mathbf{R}_2 = [\mathbf{S}_2 \ \mathbf{S}_3]^T$ . Substituting (11) into (10), we obtain

$$[\mathbf{H}^H \mathbf{\Pi}_a \ \mathbf{H}^H \mathbf{\Pi}_i] = [\mathbf{H}_a^H \ \mathbf{H}_i^H] = [\mathbf{Q}\mathbf{R}_1 \ \mathbf{Q}\mathbf{R}_2], \quad (12)$$

in which  $\mathbf{\Pi} = [\mathbf{\Pi}_a \ \mathbf{\Pi}_i]$ . In (12), the left hand side and right hand side of (10) are separated into two blocks and thus we can interpret  $\mathbf{H}_a^H$  and  $\mathbf{H}_i^H$  as the MIMO-FAS channels of active and inactive ports, respectively. Since the singular values of  $\mathbf{H}^H$  and  $\mathbf{R}$  remain the same, it is clear that (12) provides the following properties

$$\begin{aligned} \prod_{m=1}^{N_{\min}} \sigma_m(\mathbf{H}^H) &= \prod_{m=1}^{n_s} \sigma_m(\mathbf{H}_a^H) \prod_{m=n_s+1}^{N_{\min}} \sigma_m(\mathbf{H}_i^H) \\ &= \prod_{m=1}^{n_s} \sigma_m(\mathbf{R}_1) \prod_{m=n_s+1}^{N_{\min}} \sigma_m(\mathbf{R}_2), \end{aligned} \quad (13)$$

<sup>5</sup>The relaxation is done because  $R(\mathbf{A}, \mathbf{W}, \mathbf{P}) \approx \log \det(\bar{\mathbf{H}}\mathbf{K}\bar{\mathbf{H}}^H)$  at high SNR and the rate of using equal power allocation approaches to that of waterfilling power allocation as SNR increases [37]. For other SNR regimes, solving (7) with low complexity remains open. Nevertheless, we can obtain an efficient solution at low SNR by activating  $n_{rx}/n_{tx}$  ports where the row/column-norm of  $\mathbf{H}$  are the largest and they are separated by at least  $c_{rx}/c_{tx}$  distance. We refer this scheme as the greedy selection.

where  $N_{\min} = \min \{N_{rx}, N_{tx}\}$  and  $\sigma_m(\cdot)$  denotes the  $m$ -th singular value of the matrix argument.

In alignment with (9), our objective here is to maximize  $\prod_{m=1}^{n_s} \sigma_m(\mathbf{H}_a^H)$  in (13) by permuting the  $k$ -th column of  $\mathbf{H}_a^H$  and the  $l$ -th column of  $\mathbf{H}_i^H$ . To facilitate this objective, we employ the matrix  $\Omega$  where the  $(k, l)$ -th entry of  $\Omega$  is

$$\Omega_{k,l} = \sqrt{\left| \mathbf{S}_1^\dagger \mathbf{S}_2 \right|_{k,l}^2 + \|\mathbf{s}_{3,l}\|_2^2 + \left\| \mathbf{s}_{1,k}^{\dagger,T} \right\|_2^2}, \quad (14)$$

where  $|\mathbf{S}|_{k,l}$  gives the absolute value of the  $(k, l)$ -th entry of  $\mathbf{S}$ ,  $\mathbf{s}_{s,l}$  is the  $l$ -th column of  $\mathbf{S}_s$  and  $\mathbf{s}_{s,k}^{\dagger,T}$  is the  $k$ -th row of  $\mathbf{S}_s^\dagger$ . Furthermore, let us denote  $\mathbf{H}_{a,k,l}^H$  (or  $\mathbf{\Pi}_{a,k,l}$ ) as the new matrix where the  $k$ -th column of  $\mathbf{H}_a^H$  (or  $\mathbf{\Pi}_a$ ) and the  $l$ -th column of  $\mathbf{H}_i^H$  (or  $\mathbf{\Pi}_i$ ) are permuted.

Conventionally, it is necessary to permute all the  $(k, l)$  combinations and find the maximum  $\prod_{m=1}^{n_s} \sigma_m(\mathbf{H}_{a,k,l}^H)$  in the presence of spatial correlation. Nevertheless, using (14), we can determine the increase or decrease of  $\prod_{m=1}^{n_s} \sigma_m(\mathbf{H}_{a,k,l}^H)$  over  $\prod_{m=1}^{n_s} \sigma_m(\mathbf{H}_a^H)$  before permuting them. Hence, we can directly permute the  $k$ -th column of  $\mathbf{H}_a^H$  (and  $\mathbf{\Pi}_a$ ) and the  $l$ -th column of  $\mathbf{H}_i^H$  (and  $\mathbf{\Pi}_i$ ) and then update  $\mathbf{H}^H = \mathbf{H}_{a,k,l}^H$  (and  $\mathbf{\Pi} = \mathbf{\Pi}_{a,k,l}$ ) if  $\Omega_{k,l} > 1$ . In this paper, we permute the columns based on the largest  $\Omega_{k,l}$  which yields a suboptimal solution. Furthermore, we perform QR factorization to obtain the expression in (10) with the existing  $\mathbf{\Pi}$ . These steps can be repeated until  $\Omega_{k,l} \leq 1 \forall k, l$ . Using strong RRQR factorization, we can obtain  $\mathbf{H}_a^H$  with the maximum  $\prod_{m=1}^{n_s} \sigma_m(\mathbf{H}_a^H)$  where  $\mathbf{A}_{rx}^* = \mathbf{\Pi}_a^T$ . Reapplying strong RRQR factorization on  $\mathbf{A}_{rx}^* \mathbf{H}$ , we can also obtain  $\mathbf{A}_{tx}^*$  where  $\mathbf{A}_{tx}^* = \mathbf{\Pi}_a$ .

Given  $\mathbf{A}^*$ , (7) reduces to the optimal beamforming and power allocation problem which can be formulated as

$$\max_{\mathbf{W}, \mathbf{P}} R(\mathbf{W}, \mathbf{P} | \mathbf{A}^*) \quad \text{s.t.} \quad (7e), (7f). \quad (15)$$

Interestingly, (15) can be easily solved via SVD and waterfilling power allocation [27]. In particular, the solution to (15) is  $\mathbf{W}_r^* = \bar{\mathbf{M}}^H$  and  $\mathbf{W}_t^* = \bar{\mathbf{N}}$  where  $\bar{\mathbf{H}} = \bar{\mathbf{M}} \bar{\Sigma} \bar{\mathbf{N}}^H$ ,  $\bar{\mathbf{M}}$  is the left singular matrix of  $\bar{\mathbf{H}}$ ,  $\bar{\mathbf{N}}$  is the right singular matrix of  $\bar{\mathbf{H}}$ ,  $\bar{\Sigma} = \text{diag}(\bar{\Sigma}_1, \dots, \bar{\Sigma}_{n_{\min}})$  denotes the diagonal matrix whose  $l$ -th entry is the  $l$ -th singular value of  $\bar{\mathbf{H}}$ ,  $\bar{\Sigma}_1 \geq \dots \geq \bar{\Sigma}_{n_{\min}}$  and  $n_{\min} = \min \{n_{tx}, n_{rx}\}$ . In addition,  $\mathbf{P}^* = \text{diag}(p_1^*, \dots, p_{n_{\min}}^*)$ ,  $p_l^* = \left[ \mu - \frac{1}{\bar{\Sigma}_l^2} \right]_0^+$ , and  $\text{SNR} = \sum p_l^*$ . Thus, the optimal input covariance is  $\mathbf{K}^* = \mathbf{W}_{tx}^* \mathbf{P}^* \mathbf{W}_{tx}^{*H}$ . Using the above methods, the rate of the QR MIMO-FAS for a given SNR can be expressed as

$$R_{\text{QR}}(\text{SNR}) = \sum_{l=1}^{n_{\min}} \log(1 + p_l^* \bar{\Sigma}_l^2), \quad (16)$$

where (16) is useful for analyzing the optimal DMT of MIMO-FAS.

---

**Algorithm 1** Pseudocode of QR MIMO-FAS
 

---

- 1: Compute (10) via QR factorization with pivoted column
  - 2: Compute  $\Omega$  using (14)
  - 3: **While**  $\Omega_{k,l} > 1$
  - 4: Permute the  $k$ -th column of  $\mathbf{H}_a^H/\mathbf{\Pi}_a$  and the  $l$ -th column of  $\mathbf{H}_i^H/\mathbf{\Pi}_i$  with the largest  $\Omega_{k,l} > 1$
  - 5: Update  $\mathbf{H}^H = \mathbf{H}_{a,k,l}^H$  and  $\mathbf{\Pi} = \mathbf{\Pi}_{a,k,l}$
  - 6: Perform QR factorization using  $\mathbf{\Pi}$  and return to Step 2
  - 7: **end**
  - 8: Set  $\mathbf{A}_r^* = \mathbf{\Pi}_a^T$
  - 9: Repeat Steps 1–7 by replacing  $\mathbf{H}^H$  with  $\mathbf{A}_r^* \mathbf{H}$
  - 10: Set  $\mathbf{A}_t^* = \mathbf{\Pi}_a^T$
  - 11: Compute SVD on  $\mathbf{A}_r^* \mathbf{H} \mathbf{A}_t^*$  to obtain  $\mathbf{W}^*$
  - 12: Use bisection to obtain  $\mathbf{P}^*$
- 

The pseudocode of proposed scheme is presented in Algorithm 1. Let us denote  $N_{\max} = \max\{N_{tx}, N_{rx}\}$  and  $n_{\max} = \max\{n_{tx}, n_{rx}\}$ . The worst computational cost of Step 1 is  $\frac{4}{3}n_{\max}^3 - 4N_{\max}n_{\max}^2 + 4N_{\max}^2n_{\max}$  flops [30]. Steps 2–7 require  $(1 + t_i) \left[ \left( \frac{2}{3}n_{\max}^3N_{\max}^2 + 2n_{\max}^2N_{\max}^3 + 2N_{\max}^3 \right) \right]$  flops [31], where  $t_i$  is a finite number of permutations and it is usually small due to Step 1 [28]. Step 9 has the same total computational cost as Steps 1–7, which is also finite. In addition, Steps 11 and 12 require  $21n_{\max}^3$  and  $\log\left(\frac{\mu_{\max}}{\epsilon_0}\right)n_{\max}$  flops, respectively, where  $\mu_{\max}$  is the interval for searching  $\mu$  and  $\epsilon_0$  is the tolerance for bisection method. Summing up the computational costs, the proposed scheme has a polynomial time complexity of  $\mathcal{O}(n_{\max}^3N_{\max}^3)$ . Compared to the global optimal solution, the proposed scheme significantly reduces the time complexity.

#### IV. OPTIMAL DMT

In this section, we analyze the optimal DMT of MIMO-FAS. As defined in [24], a MIMO scheme is said to achieve a multiplexing gain of  $r$  and a diversity gain of  $d$  if

$$\lim_{\text{SNR} \rightarrow \infty} \frac{R_{\text{sys}}(\text{SNR})}{\log \text{SNR}} = r, \quad (17)$$

and the outage probability satisfies<sup>6</sup>

$$\lim_{\text{SNR} \rightarrow \infty} \frac{\log (P_{\text{sys}}^{\text{out}}(\text{SNR}, r))}{\log \text{SNR}} = -d(r), \quad (18)$$

in which  $R_{\text{sys}}(\text{SNR})$  and  $P_{\text{sys}}^{\text{out}}(\text{SNR}, r)$  are, respectively, the rate and outage probability of the system. Similar to [24], we use the symbol  $\doteq$  to denote exponential equality. In particular,  $f(\text{SNR}) \doteq \text{SNR}^{-d}$  if

$$\lim_{\text{SNR} \rightarrow \infty} \frac{\log (f(\text{SNR}))}{\log \text{SNR}} = -d. \quad (19)$$

To obtain the optimal DMT of MIMO-FAS, we present the following lemmas.

**Lemma 1.** *Given a 2D space with an area of  $W_s$  where both  $W_1^s \gg 0$  and  $W_2^s \gg 0$ ,  $\mathbf{J}_s$  in (2) can be represented by  $\mathbf{J}_{\text{red}}^s$ , i.e., a full rank symmetric  $N_s' \times N_s'$  finite-size matrix even if  $N_s \rightarrow \infty$ .*

*Proof:* For a positive  $W_s$ , consider (2) where  $N_s \rightarrow \infty$ . Without loss of generality, we focus on two neighboring ports: the  $(n_1^s, n_2^s)$ -th and  $(\tilde{n}_1^s, \tilde{n}_2^s)$ -th port. In cases where  $N_1^s \rightarrow \infty$ , we analyze  $(\tilde{n}_1^s, \tilde{n}_2^s) = (n_1^s + 1, n_2^s)$ . The spatial correlation between the  $(n_1^s, n_2^s)$ -th and  $(\tilde{n}_1^s, n_2^s)$ -th port is given by

$$J_{(n_1^s, n_2^s), (\tilde{n}_1^s, n_2^s)}^s = \lim_{N_1^s \rightarrow \infty} \delta_s^2 j_0 \left( \frac{2\pi}{N_1^s - 1} W_1^s \right) = \delta_s^2, \quad (20)$$

since  $\lim_{N_1^s \rightarrow \infty} \frac{1}{N_1^s - 1} = 0$ . In other words, the spatial correlation of the  $\tilde{n}_1^s$ -th port is identical to that of the  $n_1^s$ -th port. For ease of exposition, let us refer to the spatial correlation of a port as an entry.

For  $n_2^s = \{1, \dots, N_2^s\}$ , we can remove the identical entries (e.g.,  $\tilde{n}_1^s$  for  $\exists n_1^s$ ) and obtain  $\bar{N}_1^s$  distinct entries. Since  $W_1^s \gg 0$ , there is an  $\varepsilon$  such that

$$\varepsilon = \inf \left\{ e \mid \begin{array}{l} J_{(n_1^s, n_2^s), (n_1^s + e, n_2^s)}^s \neq \delta_s^2, \\ e \in \mathbb{Z}, \\ 0 < e \leq N_1^s - 1 \end{array} \right\}. \quad (21)$$

Define  $c_1^s \triangleq \frac{\varepsilon}{N_1^s - 1} W_1^s$  as the smallest spacing required for the spatial correlation between the  $(n_1^s, n_2^s)$ -th and  $(\tilde{n}_1^s, n_2^s)$ -th ports to be distinct. Then we can verify that  $\bar{N}_1^s$  is finite since  $W_1^s \geq \bar{N}_1^s c_1^s > 0$ . Let us write the  $\bar{N}_1^s$  distinct entries as a vector  $\mathbf{v}_{n_2^s}$  for each  $n_2^s \in \{1, \dots, N_2^s\}$ . If these vectors are linearly dependent, then we can similarly remove the dependent vectors and

<sup>6</sup>Here, we use the fact that the error probability can be arbitrary close to the outage probability [32], [33].

obtain  $\bar{N}_2$  independent vectors. As a result, we can rewrite  $\mathbf{J}_s$  as a symmetric  $\bar{N}_s \times \bar{N}_s$  finite-size matrix with distinct entries where  $\bar{N}_s = \bar{N}_1^s \bar{N}_2^s$ .

Using a similar argument, we see that  $\mathbf{J}_s$  can be represented by an  $\bar{N}_s \times \bar{N}_s$  finite-size matrix if  $N_2^s \rightarrow \infty$ . Combining the two cases, it is straightforward to see that  $\mathbf{J}_s$  can be rewritten as a symmetric  $\bar{N}_s \times \bar{N}_s$  matrix as  $N_1^s \rightarrow \infty$  and  $N_2^s \rightarrow \infty$  since both  $W_1^s \gg 0$  and  $W_2^s \gg 0$ , and we have (21) and

$$\varepsilon_2 = \inf \left\{ e \left| J_{(n_1^s, n_2^s), (n_1^s, n_2^s + e)}^s \neq \delta_s^2, \begin{array}{l} e \in \mathbb{Z}, \\ 0 < e \leq N_2^s - 1 \end{array} \right. \right\}. \quad (22)$$

From the above, it is clear that we can use the same argument to show that  $\mathbf{J}_s$  can be rewritten as a symmetric  $\bar{N}_s \times \bar{N}_s$  matrix if  $N_1^s/N_2^s$  is finite since we can always remove the entries where their vertical/horizontal distances between the adjacent ports are less than  $c_1^s/c_2^s$ .

Let us denote  $N'_s$  as the full rank of the symmetric  $\bar{N}_s \times \bar{N}_s$  matrix where  $N'_s \leq \bar{N}_s$ . Then we can further reduce the symmetric  $\bar{N}_s \times \bar{N}_s$  matrix to a full rank symmetric  $N'_s \times N'_s$  submatrix  $\mathbf{J}_{\text{red}}^s$  by removing the  $(\bar{N}_s - N'_s)$  dependent rows and columns. Thus,  $\mathbf{J}_s$  can always be represented by  $\mathbf{J}_{\text{red}}^s$ , i.e., a full rank symmetric  $N'_s \times N'_s$  finite-size matrix. In other words, it suffices to consider  $\mathbf{J}_{\text{red}}^s$  instead of  $\mathbf{J}_s$  since some rows/columns of  $\mathbf{J}_s$  are identical or a linear combination of the others. A more generalized result is given in Appendix II. ■

**Lemma 2.** *If  $\mathbf{J}_{tx}$  and  $\mathbf{J}_{rx}$  are full rank, the optimal DMT of any MIMO system with channel  $\mathbf{H}$  is the same as that of a system with channel  $\mathbf{G}$ .*

*Proof:* See [34]. ■

**Lemma 3.** *The optimal DMT of using only  $n_{rx} \times n_{tx}$  channels from the MIMO channel  $\mathbf{G}$ , where  $n_{tx} \leq N_{tx}$  and  $n_{rx} \leq N_{rx}$ , is a piecewise linear function connecting the points  $(n_{\min}, 0)$  and*

$$\{r, (N_{rx} - r)(N_{tx} - r)\}, \quad r = 0, \dots, N, \quad (23)$$

where

$$N = \arg \min_{\substack{\eta \in \mathbb{Z} \\ 0 \leq \eta \leq n_{\min} - 1}} \frac{(N_{rx} - \eta)(N_{tx} - \eta)}{n_{\min} - \eta}. \quad (24)$$

*Proof:* See [35]. ■

**Corollary 1.** *If the antennas are placed based on a grid structure with at least half a wavelength apart and the transmit/receive spatial correlation matrices are full rank, then the optimal DMT of*

$n_{rx} \times n_{tx}$  MIMO antenna selection is a piecewise linear function connecting the points  $(n_{\min}, 0)$  and

$$\{r, (w_{rx} - r)(w_{tx} - r)\}, \quad r = 0, \dots, N_{as}, \quad (25)$$

where

$$N_{as} = \arg \min_{\substack{\eta \in \mathbb{Z} \\ 0 \leq \eta \leq n_{\min} - 1}} \frac{(w_{rx} - \eta)(w_{tx} - \eta)}{n_{\min} - \eta}. \quad (26)$$

*Proof:* Given a fixed  $W_s^1$  and  $W_s^2$ , there can be at most  $w_s = \left(\left\lfloor \frac{W_s^1}{0.5} \right\rfloor + 1\right) \left(\left\lfloor \frac{W_s^2}{0.5} \right\rfloor + 1\right)$  antennas at side  $s$ . Using Lemma 2 and Lemma 3, we obtain (25) and (26). ■

Using the above lemmas, we can now obtain the outer bound of the DMT of MIMO-FAS.

**Theorem 1.** For finite  $W_{rx}$  and  $W_{tx}$ , the outer bound of the DMT of MIMO-FAS is a piecewise linear function connecting the points  $(n_{\min}, 0)$  and

$$\{r, (N'_{rx} - r)(N'_{tx} - r)\}, \quad r = 0, \dots, N', \quad (27)$$

where

$$N' = \arg \min_{\substack{\eta \in \mathbb{Z} \\ 0 \leq \eta \leq n_{\min} - 1}} \frac{(N'_{rx} - \eta)(N'_{tx} - \eta)}{n_{\min} - \eta}. \quad (28)$$

*Proof:* By using SVD, we can decompose  $\mathbf{H} = \mathbf{M}\mathbf{\Sigma}\mathbf{N}$  where  $\mathbf{M}$  is the left singular matrix of  $\mathbf{H}$ ,  $\mathbf{N}$  is the right singular matrix of  $\mathbf{H}$ ,  $\mathbf{\Sigma} = \text{diag}(\Sigma_1, \dots, \Sigma_{N_{\min}})$  is a diagonal matrix whose  $l$ -th entry is the singular value of  $\mathbf{H}$  and  $\Sigma_1 \geq \dots \geq \Sigma_{N_{\min}}$ . According to the Cauchy's Interlacing theorem [36], it follows that  $\Sigma_1 \geq \bar{\Sigma}_1 \geq \dots \geq \bar{\Sigma}_{n_{\min}} \geq \Sigma_{n_{\min}} \geq \dots \geq \Sigma_{N_{\min}}$ . Therefore, the rate of MIMO-FAS can be upper bounded by

$$R(\text{SNR}) = \sum_{l=1}^{n_{\min}} \log(1 + \tilde{p}_l^* \Sigma_l^2), \quad (29)$$

where  $\tilde{p}_l^* = \left[\mu - \frac{1}{\Sigma_l^2}\right]_0^+$  and  $\text{SNR} = \sum \tilde{p}_l^*$ . At high SNR, (29) can be simplified as

$$R(\text{SNR}) = \sum_{l=1}^{n_{\min}} \log\left(1 + \frac{\text{SNR}}{n_{\min}} \Sigma_l^2\right), \quad (30)$$

since the rate of using equal power allocation approaches to that of waterfilling power allocation as SNR increases [37]. Consequently, the outage probability of MIMO-FAS can be lower bounded by

$$P_{\text{out}}(\text{SNR}, r) = \mathbb{P}\{R(\text{SNR}) < r \log \text{SNR}\}. \quad (31)$$



At high SNR, the outage probability is rewritten as [24]

$$P_{\text{out}}(\text{SNR}, r) = \mathbb{P} \left\{ \sum_{l=1}^{n_{\min}} \log(1 + \text{SNR} \Sigma_l^2) < r \log \text{SNR} \right\}, \quad (32)$$

since

$$\begin{aligned} & \lim_{\text{SNR} \rightarrow \infty} \frac{\log \left( \mathbb{P} \left\{ \sum_{l=1}^{n_{\min}} \log \left( 1 + \frac{\text{SNR}}{n_{\min}} \Sigma_l^2 \right) < r \log \text{SNR} \right\} \right)}{\log \text{SNR}} \\ &= \lim_{\text{SNR} \rightarrow \infty} \frac{\log \left( \mathbb{P} \left\{ \sum_{l=1}^{n_{\min}} \log \left( 1 + \frac{\text{SNR}}{n_{\min}} \Sigma_l^2 \right) < r \log \text{SNR} \right\} \right)}{\log \frac{\text{SNR}}{n_{\min}}} \\ &= \lim_{\text{SNR} \rightarrow \infty} \frac{\log \left( \mathbb{P} \left\{ \sum_{l=1}^{n_{\min}} \log(1 + \text{SNR} \Sigma_l^2) < r \log \text{SNR} \right\} \right)}{\log \text{SNR}}. \end{aligned} \quad (33)$$

Using (19), we can obtain the outer bound on the diversity gain for a fixed multiplexing gain  $r$  as

$$P_{\text{out}}(\text{SNR}, r) \doteq \mathbb{P} \left\{ \sum_{l=1}^{n_{\min}} \log(1 + \text{SNR} \Sigma_l^2) < r \log \text{SNR} \right\}. \quad (34)$$

According to [38], the joint probability density function (PDF) of  $\Sigma^2$  is given by

$$f(\Sigma^2) = \sum_{\mathbf{q}} \frac{(-1)^{\frac{N_{\min}(N_{\min}-1)}{2}} \mathcal{A}}{N_{\min}! \Delta(\mathbf{q})} \Delta(\Sigma^2) \det \left( \Sigma_k^{2(q_l + N_{\max} - N_{\min})} \right), \quad (35)$$

where  $\mathbf{q} = [q_1, \dots, q_{N_{\max}}]^T$ ,  $N_{\min} = \min \{N_{tx}, N_{rx}\}$ ,

$$\mathcal{A} = \frac{\prod_{k=1}^{N_{\min}} \lambda_k^s \prod_{l=1}^{N_{\max}} \lambda_l^{s'} \det \left( (-\lambda_k^s)^{q_l} \right) \det \left( (\lambda_k^{s'})^{q_l + N_{\max} - N_{\min}} \Big|_{k=1}^{N_{\min}}, (\lambda_l^{s'})^{N_{\max} - k} \Big|_{k=N_{\min}+1}^{N_{\max}} \right)}{\Delta(\boldsymbol{\lambda}^s) \Delta(\boldsymbol{\lambda}^{s'}) \prod_{l=1}^{N_{\min}} (q_l + N_{\max} - N_{\min})!}, \quad (36)$$

where

$$\begin{cases} s = \{s | N_s = \min \{N_{tx}, N_{rx}\}\}, \\ s' = \{s' | N_{s'} = \max \{N_{tx}, N_{rx}\}\}, \\ \boldsymbol{\lambda}^s = [\lambda_1^s, \dots, \lambda_{N_s}^s]^T, \end{cases} \quad (37)$$

$\Delta(\boldsymbol{\lambda}^s)$  denotes the Vandermonde determinant of vector  $\boldsymbol{\lambda}^s$ ,  $\det(f(k, l))$  is the determinant of a matrix with the  $(k, l)$ -th entry given by the function  $f(k, l)$  and  $q_l = b_l + N_{\max} - l$ . In addition,  $\mathbf{b} = [b_1, \dots, b_{N_{\max}}]^T$  is the irreducible representation of unitary group such that  $b_1 \geq \dots \geq b_{N_{\max}} \geq 0$  are integers.

Conventionally, we can analyze the outer bound by simplifying the joint PDF of  $\Sigma^2$  and then analyzing the exponents of  $\Sigma_l$ . Nevertheless, it is found that no simplification can be made to

keep the exponents of  $\Sigma_l$  tractable when the rows and columns of  $\mathbf{H}$  are fully correlated [39]. To alleviate this problem, we employ Lemma 1, Lemma 2, and Lemma 3.

Specifically, according to [40], the PDF of  $\mathbf{H}$  can be obtained by removing the dependent entries and the PDF of the singular values of  $\mathbf{H}$  can be obtained via coordinate changes [41]. Using Lemma 1, we know that  $\mathbf{J}_s$  can be represented by a full rank symmetric finite-size matrix, i.e.,  $\mathbf{J}_{\text{red}}^s \in \mathbb{R}^{N'_s \times N'_s}$  and  $\text{rank}(\mathbf{J}_{\text{red}}^s) = N'_s$ . It follows that  $\mathbf{H}$  and  $\mathbf{G}$  in (3) can be rewritten as  $N'_{rx} \times N'_{tx}$  matrices with the same PDFs. From Lemma 2, it is known that the DMT of any MIMO system with channel  $\mathbf{H} \in \mathbb{C}^{N'_{rx} \times N'_{tx}}$  is the same as that of a system with channel  $\mathbf{G} \in \mathbb{C}^{N'_{rx} \times N'_{tx}}$ . Since  $\mathbf{G}$  is an independent and identically distributed (i.i.d.) circularly symmetric complex Gaussian matrix, it follows that  $\text{rank}(\mathbf{G}) = N'_{\min} = \min\{N'_{rx}, N'_{tx}\}$  with probability one. Using Lemma 3, we can conclude that the outer bound of the DMT of MIMO-FAS is a piecewise linear function connecting the points as given in (27) and (28). ■

Using Theorem 1, we can now derive the optimal DMT of MIMO-FAS by considering its outer bound and inner bound. Specifically, the DMT of QR MIMO-FAS can be regarded as the inner bound of the DMT of MIMO-FAS.

**Theorem 2.** *The DMT of QR MIMO-FAS is equivalent to the outer bound of the DMT of MIMO-FAS, and thus it is also the optimal DMT of MIMO-FAS.*

*Proof:* At high SNR, (16) can be simplified as

$$R_{\text{QR}}(\text{SNR}) = \sum_{l=1}^{n_{\min}} \log \left( 1 + \frac{\text{SNR}}{n_{tx}} \bar{\Sigma}_l^2 \right) \quad (38)$$

since the rate of using equal power allocation approaches to that of waterfilling power allocation as SNR increases [37]. Consequently, the outage probability is characterized by

$$P_{\text{QR}}^{\text{out}}(\text{SNR}, r) = \mathbb{P} \{ R_{\text{QR}}(\text{SNR}) < r \log \text{SNR} \}. \quad (39)$$

At high SNR, the difference between (30) and (38) is

$$R(\text{SNR}) - R_{\text{QR}}(\text{SNR}) \approx \sum_{l=1}^{n_{\min}} \log \left( \frac{n_{tx} \Sigma_l^2}{n_{\min} \bar{\Sigma}_l^2} \right) = c_0, \quad (40)$$

which is a constant.<sup>7</sup> As  $\lim_{c \rightarrow \infty} \log\left(\frac{1+c}{c}\right) = 0$ , the approximation of (40) is tight as  $\text{SNR} \rightarrow \infty$ .

As such, we have

$$\begin{aligned} \lim_{\text{SNR} \rightarrow \infty} \frac{R_{\text{QR}}(\text{SNR})}{\log \text{SNR}} &= \lim_{\text{SNR} \rightarrow \infty} \frac{R(\text{SNR}) - c_0}{\log \text{SNR}} \\ &= \lim_{\text{SNR} \rightarrow \infty} \frac{R(\text{SNR})}{\log \text{SNR}}, \end{aligned} \quad (41)$$

and

$$\begin{aligned} &\lim_{\text{SNR} \rightarrow \infty} \frac{\log(P_{\text{QR}}^{\text{out}}(\text{SNR}, r))}{\log \text{SNR}} \\ &= \lim_{\text{SNR} \rightarrow \infty} \frac{\log(\mathbb{P}\{R(\text{SNR}) < r \log \text{SNR} + c_0\})}{\log \text{SNR}} \\ &= \lim_{\text{SNR} \rightarrow \infty} \frac{\log(\mathbb{P}\{R(\text{SNR}) < r \log \text{SNR}\})}{\log \text{SNR}} \\ &= \lim_{\text{SNR} \rightarrow \infty} \frac{\log(P_{\text{out}}(\text{SNR}, r))}{\log \text{SNR}}. \end{aligned} \quad (42)$$

Thus, the DMT of QR MIMO-FAS is equivalent to the outer bound, and also the optimal DMT of MIMO-FAS.  $\blacksquare$

It is challenging to explicitly obtain  $N'_s$  because  $\mathbf{J}_s$  might be near to being singular. It is also unclear how  $\mathbf{J}_s$  can be reduced to/reconstructed from  $\mathbf{J}_{\text{red}}^s$ . To address these issues, we propose methods to reliably estimate  $N'_s$ , and to linearly transform  $\mathbf{J}_s$  to  $\mathbf{J}_{\text{red}}^s$  and vice versa with a proof of certificates. These methods are based on the following theorems.

**Theorem 3.** *Since  $\mathbf{J}_s$  can be well-approximated by  $\hat{\mathbf{J}}_s$  where  $\hat{\mathbf{J}}_s = \mathbf{U}_s \hat{\mathbf{\Lambda}} \mathbf{U}_s^H$  and  $\hat{\mathbf{\Lambda}} = \text{diag}(\lambda_1^s, \dots, \lambda_{N'_s}^s, 0, \dots, 0)$ , the rank of  $\mathbf{J}_s$  can be estimated as  $N'_s$ .*

*Proof:* Define an arbitrarily small  $\xi > 0$  as the threshold where the numerical values of the eigenvalues are negligible. According to [42],  $\mathbf{J}_s$  can be regularized by  $\hat{\mathbf{J}}_s$ , where  $\hat{\mathbf{J}}_s = \mathbf{U}_s \hat{\mathbf{\Lambda}} \mathbf{U}_s^H$ ,  $\hat{\mathbf{\Lambda}} = \text{diag}(\lambda_1^s, \dots, \lambda_{N'_s}^s, 0, \dots, 0)$  and  $\lambda_l^s < \xi$ ,  $l \in \{N'_s + 1, \dots, N_s\}$ . The Frobenius norm between  $\mathbf{J}_s$  and  $\hat{\mathbf{J}}_s$  is given by

$$E = \|\mathbf{J}_s - \hat{\mathbf{J}}_s\|_F = \sum_{l=N'_s+1}^{N_s} \lambda_l^s, \quad (43)$$

which can be upper bounded by  $(N_s - N'_s)\xi$ . In practice, we have  $\lambda_1^s \gg \lambda_{N'_s+1}^s > \dots > \lambda_{N_s}^s$  and thus (43) is usually very small. Therefore, the rank of  $\mathbf{J}_s$  can be estimated as  $N'_s$ .  $\blacksquare$

<sup>7</sup>Note that a constant gap amounts to a finite scaling of SNR. This implies that  $R(\text{SNR}) = R_{\text{QR}}(\text{SNR} + \gamma)$  for some  $\gamma > 0$ .

Table II: Estimation of  $N'_s$  for different  $W_s$ , where  $\xi = 10^{-3}$ ,  $N_s = 100$ ,  $N_1^s = N_2^s$ , and  $W_1^s = W_2^s$ .

$W_s$	$0.5 \times 0.5$	$1 \times 1$	$1.5 \times 1.5$	$2 \times 2$	$2.5 \times 2.5$	$3 \times 3$
$N'_s$	13	23	34	48	60	73
$E$	0.001	0.002	0.003	0.002	0.005	0.005

[<sup>†</sup>] Note that the figures regarding the diversity order of MIMO-FAS described in [25] were based on an earlier version of this paper considering the spatial correlation in 2D environments only. The correct diversity orders for MIMO-FAS in 3D environments should be referred to this table. For example, for MIMO-FAS with  $0.5\lambda \times 0.5\lambda$  FAS at both ends, the diversity order is  $13 \times 13 = 169$  which is much higher than originally reported.

**Theorem 4.** For arbitrary  $N_s = N_1^s \times N_2^s$  and a finite  $W_s = W_1^s \times W_2^s$ ,  $\mathbf{J}_s$  in (2) can be reduced to  $\mathbf{J}_{\text{red}}^s$  using the set  $\mathcal{V}_s = \{\mathbf{v}_l^s | \mathbf{J}_s^{(l)} \tilde{\mathbf{v}}_l^s = \mathbf{0}, l = N'_s + 1, \dots, N_s\}$  where  $\tilde{\mathbf{v}}_l^s = [\mathbf{v}_l^s \ -1]^T$ . Conversely,  $\mathbf{J}_s$  in (2) can be reconstructed from  $\mathbf{J}_{\text{red}}^s$  with the set  $\mathcal{V}_s$ .

*Proof:* Let us introduce a vector  $\tilde{\mathbf{v}}_l^s = [\mathbf{v}_l^s \ -1]^T$  where  $\mathbf{v}_l^s \in \mathbb{R}^l$  and  $\mathbf{v}_l^s \neq \mathbf{0}$ . In addition, let us denote

$$\mathbf{J}_s^{(l)} = \begin{bmatrix} \mathbf{J}_{\text{sub}}^{(l-1)} & \mathbf{j}_l \\ \mathbf{j}_l^T & j_{l,l} \end{bmatrix}. \quad (44)$$

Note that  $\mathbf{J}_s = \mathbf{J}_s^{(N_s)}$  and  $\mathbf{J}_{\text{red}}^s = \mathbf{J}_s^{(N'_s)}$ . If  $N'_s = N_s$ , then  $\mathcal{V}_s$  is an empty set and  $\mathbf{J}_s = \mathbf{J}_{\text{red}}^s$ . Thus, we can focus on the case where  $N'_s < N_s$ . Without loss of generality, we may assume that the last column of  $\mathbf{J}_s^{(l)}$  is a linear combination of the first  $(l-1)$  columns of  $\mathbf{J}_s^{(l)}$ . This implies that  $\mathbf{J}_s^{(l)} \tilde{\mathbf{v}}_l^s = \mathbf{0}$ , i.e.,  $\tilde{\mathbf{v}}_l^s$  is in the null space of  $\mathbf{J}_s^{(l)}$  and  $\tilde{\mathbf{v}}_l^s \neq \mathbf{0}$ . If  $\mathbf{J}_s^{(l)} \tilde{\mathbf{v}}_l^s = \mathbf{0}$  and  $l \neq N'_s$ , we can reduce  $\mathbf{J}_s^{(l)}$  to  $\mathbf{J}_{\text{sub}}^{(l-1)}$  by setting  $\mathbf{v}_l^s \in \mathcal{V}_s$ . Otherwise, we have  $\mathbf{J}_s^{(l)} = \mathbf{J}_{\text{red}}^s$  since  $\mathbf{J}_s^{(l)}$  must be a full rank matrix. Conversely,  $\mathbf{J}_s^{(l)}$  can be reconstructed from  $\mathbf{J}_{\text{sub}}^{(l-1)}$  if  $\mathbf{v}_l^s$  is given. Specifically, we can define  $\mathbf{j}_l \triangleq \mathbf{J}_{\text{sub}}^{(l-1)} \mathbf{v}_l^s$  and  $j_{l,l} \triangleq \mathbf{j}_l^T \mathbf{v}_l^s$  and they are sufficient to reconstruct  $\mathbf{J}_s^{(l)}$ . Hence,  $\mathbf{v}_l^s$  can be interpreted as a certificate that  $\mathbf{J}_s^{(l)}$  can be reduced to/reconstructed from  $\mathbf{J}_{\text{sub}}^{(l-1)}$  for  $l = \{N'_s + 1, \dots, N_s\}$ . ■

The proposed methods enable us to estimate  $N'_s$  for given  $N_1^s$ ,  $N_2^s$ ,  $W_1^s$ , and  $W_2^s$ . Furthermore, they allow us to verify that  $\mathbf{J}_s$  indeed can be reduced to (or reconstructed from)  $\mathbf{J}_{\text{red}}^s$  with proof of certificates. An example of the estimations of  $N'_s$  is given in Table II. This table can help us better understand the performance of MIMO-FAS. For example, by substituting the estimation of  $N'_s$  into Theorem 1, we observe that MIMO-FAS yields massive diversity gains if  $r < n_{\min}$ .

Thus, it is worth investigating how we can leverage MIMO-FAS effectively. To answer this question, we introduce the  $q$ -outage capacity.

**Definition 1.** The  $q$ -outage capacity of a system is defined as

$$C_{\text{sys}}^q = q \left( 1 - \bar{P}_{\text{sys}}^{\text{out}}(\text{SNR}, q) \right), \quad (45)$$

where

$$\bar{P}_{\text{sys}}^{\text{out}}(\text{SNR}, q) = \mathbb{P} \{ R_{\text{sys}}(\text{SNR}) < q \}, \quad (46)$$

where  $P_{\text{sys}}^{\text{out}}(q)$  is the outage probability of a system for a fixed target rate or transmission rate  $q$  independent of the SNR. It is worth noting that (45) differs from the  $\epsilon$ -outage capacity as it is not measuring the largest  $q$  such that  $\bar{P}_{\text{sys}}^{\text{out}}(\text{SNR}, q) \leq \epsilon$ . Instead, (45) is interpreted as the average rate that a system can reliably transmit over period of time such that the statistics of the fading do not change. Furthermore, both  $q$  and  $\bar{P}_{\text{sys}}^{\text{out}}(\text{SNR}, q)$  play important roles in (45). For example, if  $q \approx 0$ , we usually have  $\bar{P}_{\text{sys}}^{\text{out}}(\text{SNR}, q) \approx 0$ . If  $q$  is large, then we typically have  $\bar{P}_{\text{sys}}^{\text{out}}(\text{SNR}, q) \approx 1$ . Nevertheless, both cases yield  $C_{\text{sys}}^q \approx 0$ . In between the two extremes, we have  $C_{\text{sys}}^q \gg 0$  and there is an optimal  $q$  for a system such that (45) is maximized. In addition, the  $q$ -outage capacity gain of MIMO-FAS over a traditional antenna system can be characterized as

$$C_{\text{MIMO-FAS}}^q - C_{\text{sys}}^q = q \left[ \bar{P}_{\text{sys}}^{\text{out}}(\text{SNR}, q) - \bar{P}_{\text{MIMO-FAS}}^{\text{out}}(\text{SNR}, q) \right]. \quad (47)$$

Using (47), we can easily see the benefits that can be harnessed by MIMO-FAS over a traditional antenna system.

## V. RESULTS AND DISCUSSIONS

In this section, we present the analytical and Monte Carlo simulation results to evaluate the performance of MIMO-FAS. The Monte Carlo simulation results are obtained by averaging  $10^6$  independent channel realizations. For brevity, we focus on a symmetric MIMO-FAS design where  $N_1^s = N_2^s$ ,  $W_1^s = W_2^s$  and  $W_{rx} = W_{tx}$ . Unless stated otherwise, we assume that  $N_s = 100$ ,  $n_s = 4$ ,  $W_s = 1$ ,  $\delta_s^2 = 1$  and SNR = 30dB. We also consider multiple schemes based on different

combinations of techniques to highlight the respective gains and effects. These benchmarking schemes are:<sup>8</sup>

- Optimal MIMO-FAS: It considers the MIMO-FAS setup that utilizes an exhaustive search, SVD and waterfilling for port selection, beamforming and power allocation.
- QR MIMO-FAS: This is the proposed MIMO-FAS that employs strong RRQR factorization, SVD and waterfilling power allocation for a suboptimal solution.
- Greedy MIMO-FAS: This is the MIMO-FAS that employs greedy selection, SVD and waterfilling power allocation for an efficient solution in the low SNR regime.
- Random MIMO-FAS: It randomly activates the ports and uses SVD as well as waterfilling power allocation.
- MIMO: This refers to the traditional MIMO that employs SVD and waterfilling power allocation. Unless otherwise stated, we assume that the number of antennas is  $n_s^{\text{mimo}} = 4$  and the antennas are spatially correlated based on (1).
- MIMO-AS: This refers to the traditional MIMO antenna selection system that employs strong RRQR factorization, SVD and waterfilling power allocation. Unless stated otherwise, the number of active antennas is  $n_s^{\text{mimo-as}} = 4$ . Also, a maximum number of antennas is considered in the given surface where the antennas are placed based on a grid structure with at least half a wavelength apart, and they are spatially correlated due to (1).

To highlight the superiority of 2D space, we first consider a simplified scenario where there is only a single fluid antenna at the receiver. Fig. 2 shows the outage probability of FAS versus SNR for various number of ports and dimensional space. Here, the outage probability is obtained using (46) by replacing  $R_{\text{sys}}$  (SNR) with  $R_{\text{QR}}$  (SNR). Given the same number of ports, the ports that are distributed in 2D space can achieve a much lower outage probability as compared to the ones that are distributed in 1D space. This improvement can be explained from the fact that a 2D space has an additional dimension for the fluid antenna to move around. Hence, it contains more spatial diversity and yields a lower outage probability. This suggests that the ports in MIMO-FAS should be designed using the entire 2D space for better performance.

<sup>8</sup>Note that [23] has proposed a solution where the antennas can move to locally optimal positions. We can interpret these positions as activating some ports as  $N_s \rightarrow \infty$ . However, the solution cannot be employed here due to two impediments. Firstly, the spatial correlation of these positions cannot be obtained. Secondly, we are considering the cases where the positions might be discrete. Therefore, the solution is not considered in this paper.

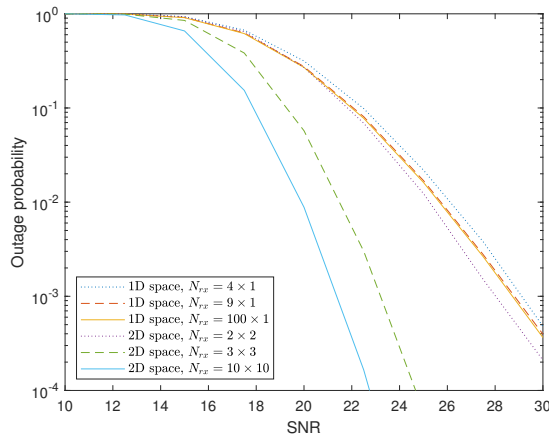
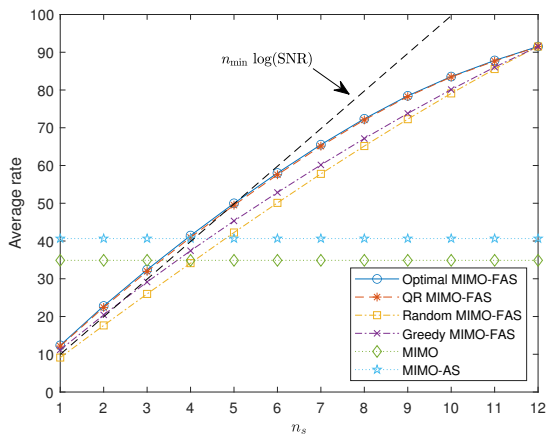


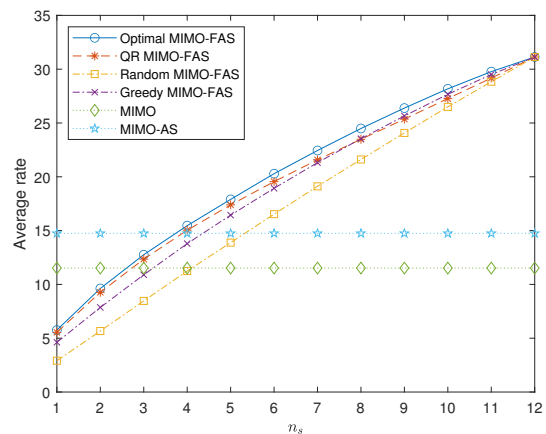
Figure 2: Outage probability of FAS versus SNR for different number of ports and dimensional space, with  $q = 7\text{bps/Hz}$ .

Next in Fig. 3, we study the average rates of the benchmarking schemes for different  $n_s$  at different SNR. Since the optimal MIMO-FAS is computed using an exhaustive search, we set  $N_s = 12$  where  $N_1^s = 4$  and  $N_2^s = 3$ . Fig. 3(a) illustrates that QR MIMO-FAS achieves a similar average rate as compared to the optimal MIMO-FAS at high SNR. Furthermore, the average rate of QR MIMO-FAS scales like  $n_s \log \text{SNR}$  when  $n_s$  ranges from 1 to 6. Nevertheless, it suffers from a diminishing rate gain when  $n_s$  ranges from 7 to 12. Thus, MIMO-FAS is most effective when each active port has the freedom of being at least half a wavelength apart from each other. In addition, the average rate of QR MIMO-FAS outperforms traditional MIMO when the number of active ports or antennas is the same (i.e.,  $n_s = 4$ ). This is because QR MIMO-FAS activates the optimal ports in each realization, which reduces the spatial correlation effect. In Fig. 3(b), we further observe that QR MIMO-FAS provides a decent performance in the medium SNR regime. Nevertheless, as shown in Fig. 3(c), greedy MIMO-FAS is more efficient than QR MIMO-FAS in the low SNR regime. Besides, QR MIMO-FAS yields a similar or higher rate than MIMO-AS when the number of active ports or antennas is the same.

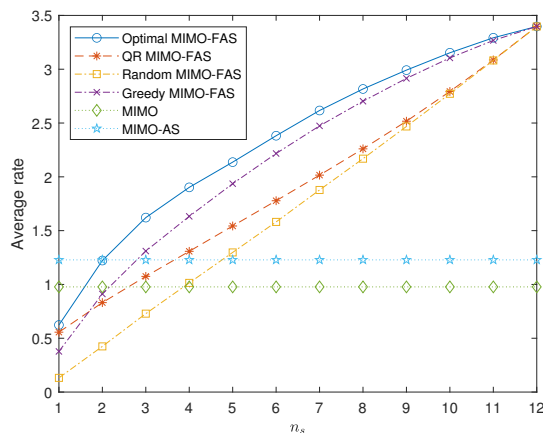
Fig. 4 presents the average rates and outage probabilities of the benchmarking schemes for different values of  $N_s$ . In these results, we omit the optimal MIMO-FAS because it is difficult to perform exhaustive search for large  $N_s$ . In Fig. 4(a), we observe that the average rates of random MIMO-FAS and greedy MIMO-FAS generally decrease as  $N_s$  increases. This suggests that efficient port selection in MIMO-FAS is essential. Furthermore, the average rate of QR



(a)



(b)



(c)

Figure 3: Average rates of the benchmarking schemes for different values of  $n_s$ : a) SNR = 30dB; b) SNR = 10dB; c) SNR = -10dB.

MIMO-FAS is 2bps/Hz higher than that of MIMO-AS and 7bps/Hz higher than that of MIMO when  $N_s$  is large.

In Fig. 4(b), the outage probabilities of random MIMO-FAS, Greedy MIMO-FAS and MIMO are near one (i.e., 0.99) while the outage probability of MIMO-AS is in the order of  $10^{-1}$ . In contrast, the outage probability of QR MIMO-FAS is much lower (i.e., the order of  $10^{-3}$ ). Nevertheless, the outage probability of QR MIMO-FAS decreases to a floor as  $N_s$  continues to increase. This limitation is due to the fact that there are approximately  $N'_s$  diversity in  $\mathbf{J}_s$  for a fixed  $W_s$ . Therefore, the outage probability of QR MIMO-FAS is limited by  $N'_s$  for a fixed  $W_s$ .



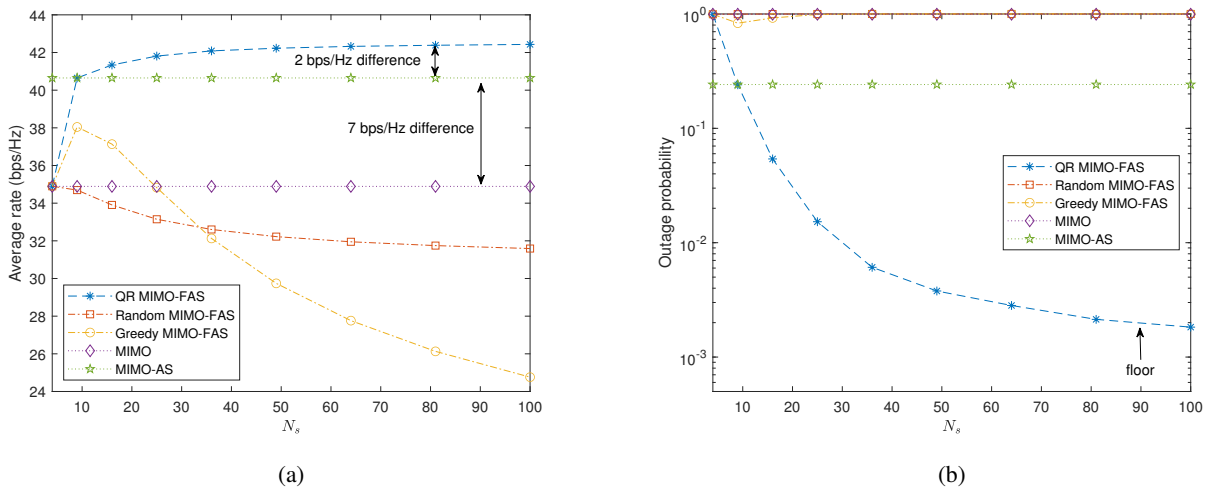


Figure 4: The performance of the benchmarking schemes for different values of  $N_s$ : (a) average rate; (b) outage probability, with  $q = 40$  bps/Hz.

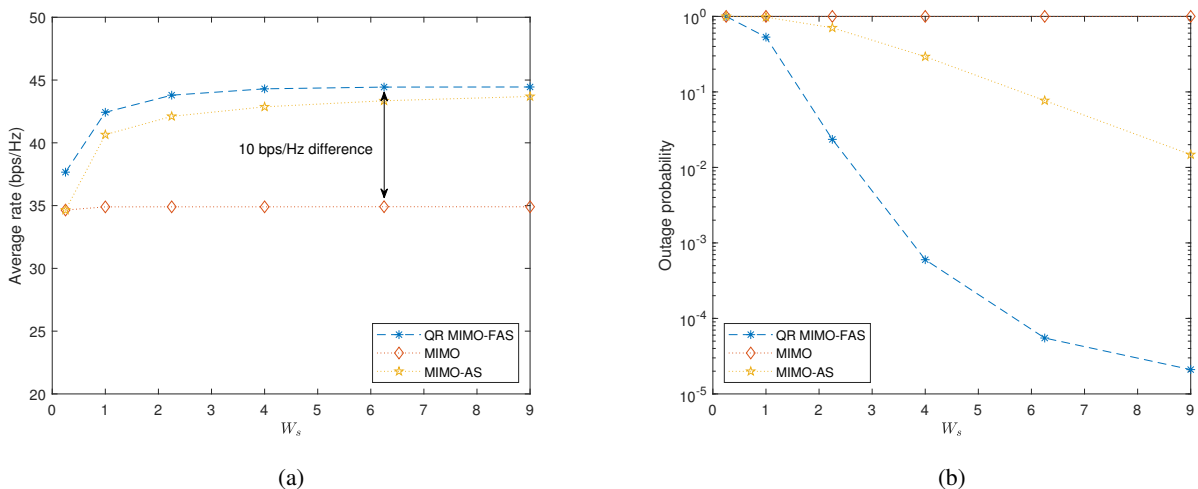


Figure 5: The performance of QR MIMO-FAS, MIMO and MIMO-AS for different values of  $W_s$ : (a) average rate; (b) outage probability, with  $q = 42.5$  bps/Hz.

(see, Table II).

To verify this explanation, we further investigate the outage probabilities of QR MIMO-FAS, MIMO and MIMO-AS for different values of  $W_s$ . For brevity, we omit random MIMO-FAS and greedy MIMO-FAS as we now know that these schemes do not provide an effective performance

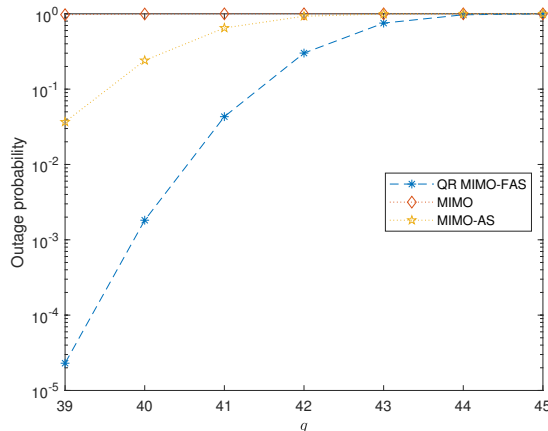


Figure 6: The outage probabilities of QR MIMO-FAS, MIMO and MIMO-AS for different values of  $q$ .

for large  $N_s$ . As seen in Fig. 5(a), the average rates of QR MIMO-FAS, MIMO and MIMO-AS increase and then plateau. Nevertheless, as shown in Fig. 5(b), the outage probabilities of QR MIMO-FAS decreases without bound as  $W_s$  increases if  $N_s$  is sufficiently large. By analyzing Table II, we can see that although  $N_s$  remains fixed,  $N'_s$  generally increases if  $W_s$  is increased. In contrast, the outage probability of MIMO is always near to being one since the diversity gain of MIMO remains the same even if  $W_s$  is increased. On the other hand, the outage probability of MIMO-AS decreases at a slower rate due to the lower resolution (i.e., the number of antennas is smaller than the number of ports in the given space). Overall, Figs. 4 and 5 suggest that the value of  $N_s$  should be determined by  $W_s$ .

From the above results, one might be amazed with the rate improvement of QR MIMO-FAS. Nevertheless, we highlight that the superiority of QR MIMO-FAS actually lies in the diversity gain. In particular, QR MIMO-FAS can reduce its outage probability to a much lower value than MIMO and MIMO-AS if  $q$  is low (e.g.,  $q < n_{\min} \log \text{SNR}$ ). To examine this phenomenon more closely, Fig. 6 illustrates the outage probabilities of QR MIMO-FAS, MIMO and MIMO-AS for different  $q$ . Within 6bits/Hz, we see that the outage probability of QR MIMO-FAS reduces at a steeper rate (e.g., from the order of  $10^{-1}$  to  $10^{-5}$ ) while the outage probability of MIMO-AS reduces at a slower rate (e.g., from the order of  $10^{-1}$  to  $10^{-2}$ ) and the outage probability of MIMO remains roughly the same.

To understand this at a more fundamental level, we present the DMT of QR MIMO-FAS in

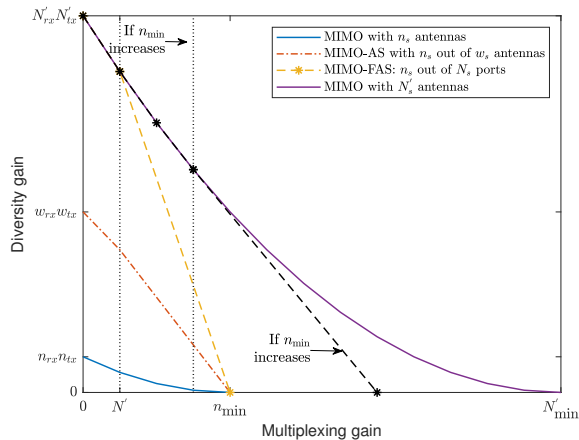


Figure 7: The optimal DMT of MIMO-FAS, MIMO and MIMO-AS.

Fig. 7. Note that the DMT of QR MIMO-FAS is also the optimal DMT of MIMO-FAS. As shown in Table II, the value of  $N'_s$  depends on  $W_s$  as long as  $N_s \geq N'_s$ . In Fig. 7, it can be seen that the diversity gain of MIMO-FAS is much superior than that of an  $n_{rx} \times n_{tx}$  MIMO system for a fixed  $r$ . For example, the maximum diversity of  $4 \times 4$  MIMO is 16 as  $r \rightarrow 0$ . This is because the optimal DMT of a traditional  $n_{rx} \times n_{tx}$  MIMO system is a piecewise linear function connecting the point  $(r, (n_{rx} - r)(n_{tx} - r))$  [24]. Meanwhile, the maximum diversity of MIMO-AS is limited by  $w_{rx}w_{tx}$ . For instance, if  $W_s = 1$ , the maximum diversity of MIMO-AS is 81. In contrast, the maximum diversity gain of MIMO-FAS is approximately  $23 \times 23 = 529 \gg \{81, 16\}$  if  $W_{rx} = W_{tx} = 1$ . Hence, the diversity gain of MIMO-FAS is massive because outage only occurs when all the ports experience deep fading. To obtain the same diversity gain at multiplexing gain  $r$  ranging from 0 to  $N'$ , a traditional  $N'_{rx} \times N'_{tx}$  MIMO would have been required. However, the downside of MIMO-FAS is that it can only have at most  $n_{\min}$  multiplexing gain.

Finally, we investigate the  $q$ -outage capacity to showcase the benefits of MIMO-FAS. Fig. 8 presents the  $q$ -outage capacities of QR MIMO-FAS, MIMO and MIMO-AS as well as the  $q$ -outage capacity gain of QR MIMO-FAS over MIMO and MIMO-AS. For ease of exposition, the optimal  $q^*$  of QR MIMO-FAS, MIMO and MIMO-AS are denoted as  $q^*_{\text{MIMO-FAS}}$ ,  $q^*_{\text{MIMO}}$ ,  $q^*_{\text{MIMO-AS}}$ , respectively. As it is seen, the outage capacities of the schemes increase up to  $q^*$  and decrease thereafter. To the left side of  $q^*$ , the capacity is limited by  $q$  (i.e., rate) since  $\bar{P}_{\text{sys}}^{\text{out}}(\text{SNR}, q)$  is small. To the right side of  $q^*$ , the capacity is limited by the outage probability because  $\bar{P}_{\text{sys}}^{\text{out}}(\text{SNR}, q)$  is large. Since MIMO provides limited diversity gain and MIMO-AS has

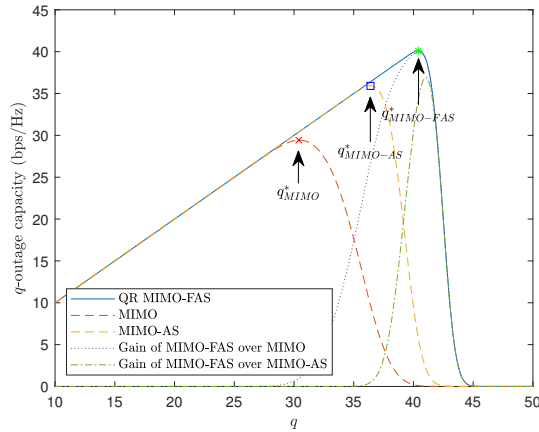


Figure 8: The  $q$ -outage capacity of MIMO-FAS, MIMO and MIMO-AS.

a limited number of antennas within a given space, both schemes fail to achieve certain  $q$ -outage capacity achievable by QR MIMO-FAS. This suggests that MIMO-FAS can reliably deliver a much higher rate than traditional MIMO and MIMO-AS systems.

## VI. CONCLUSIONS

In this paper, we analyzed the performance limits of MIMO-FAS. To this end, we developed a system model for MIMO-FAS where a 2D fluid antenna surface was used at both ends, while taking into account of the spatial correlation of the ports. We then proposed a suboptimal scheme to maximize the rate of MIMO-FAS at high SNR via joint port selection, beamforming and power allocation, namely QR MIMO-FAS. One key contribution was the derivation of the outer bound of the DMT for MIMO-FAS. Through the outer bound and the proposed scheme, we then obtained the optimal DMT of MIMO-FAS which revealed the fundamental limits of MIMO-FAS. Extensive results were presented, illustrating that QR MIMO-FAS achieved a similar rate as compared to the optimal MIMO-FAS in the high SNR regime. By fixing other MIMO-FAS parameters, we found that the average rate and outage probability of QR MIMO-FAS approached to a limit as  $N_s$  increased. Likewise, the average rate of QR MIMO-FAS improved up to a certain level as  $W_s$  increased. Nevertheless, the outage probability of QR MIMO-FAS decreased without bound as  $W_s$  increased. For the same multiplexing gain, we also showed that MIMO-FAS achieved massive diversity gain as compared to the traditional MIMO and MIMO-AS systems. Motivated by this, we further illustrated that MIMO-FAS could reliably deliver a much higher

rate than the traditional MIMO and MIMO-AS systems in terms of  $q$ -outage capacity that jointly considered both rate and outage probability.

### APPENDIX I: SPATIAL CORRELATION OF 2D FLUID ANTENNA SURFACE OVER 3D SCATTERING ENVIRONMENT

Without loss of generality, let us refer to the position of the  $(n_1, n_2)$ -port as  $\mathbf{n}_{l_s} = \left[ 0, \frac{n_2^s - 1}{N_2^s - 1} W_2^s, \frac{n_1^s - 1}{N_1^s - 1} W_1^s \right]^T$  where  $\text{map}(n_1, n_2) = l_s$  and  $\lambda$  is the wavelength. Suppose a plane wave impinges on the fluid antenna surface from azimuth angle  $\varphi$  and elevation angle  $\theta$ . Then, the array response vector can be expressed as [43]

$$\mathbf{a}(\varphi, \theta) = \left[ e^{j\frac{2\pi}{\lambda} \mathbf{k}(\varphi, \theta)^T \mathbf{n}_{1\lambda}}, \dots, e^{j\frac{2\pi}{\lambda} \mathbf{k}(\varphi, \theta)^T \mathbf{n}_{N_s \lambda}} \right]^T, \quad (48)$$

where

$$\mathbf{k}(\varphi, \theta) = \left[ \cos(\theta) \cos(\varphi) \quad \cos(\theta) \sin(\varphi) \quad \sin(\theta) \right]^T, \quad (49)$$

is the normalized wave vector.

Let us denote the spatial correlation matrix as  $\mathbf{J}_s = \delta_s^2 \mathbb{E} \left\{ \mathbf{a}(\varphi, \theta) \mathbf{a}(\varphi, \theta)^H \right\}$ . From (48), we know that the  $(k_s, l_s)$ -th entry of  $\mathbf{J}_s$  can be expressed as

$$\begin{aligned} [\mathbf{J}_s]_{k_s, l_s} &= \delta_s^2 \mathbb{E} \left\{ e^{j\frac{2\pi}{\lambda} \mathbf{k}(\varphi, \theta)^T \mathbf{n}_{k_s \lambda}} e^{-j\frac{2\pi}{\lambda} \mathbf{k}(\varphi, \theta)^T \mathbf{n}_{l_s \lambda}} \right\} \\ &= \delta_s^2 \mathbb{E} \left\{ e^{j2\pi \mathbf{k}(\varphi, \theta)^T (\mathbf{n}_{k_s} - \mathbf{n}_{l_s})} \right\}, \end{aligned} \quad (50)$$

where  $\text{map}(\tilde{n}_1^s, \tilde{n}_2^s) = k_s$ . Using the Jacobi-Anger plane wave expansion [44], (50) can be rewritten as

$$\begin{aligned} [\mathbf{J}_s]_{k_s, l_s} &= \delta_s^2 4\pi \sum_{m=0}^{\infty} \sum_{n=-m}^m (-i)^m \times \\ &\quad \alpha_m^n Y_m^n \left( \frac{\mathbf{n}_{k_s} - \mathbf{n}_{l_s}}{\|\mathbf{n}_{k_s} - \mathbf{n}_{l_s}\|} \right) \times \\ &\quad j_m(2\pi \|\mathbf{n}_{k_s} - \mathbf{n}_{l_s}\|), \end{aligned} \quad (51)$$

where  $j_m(\cdot)$  is the spherical Bessel function of the first kind,  $Y_m^n(\cdot)$  is the spherical harmonics, and

$$\alpha_m^n = \int_{\Omega} f_{\mathbf{k}(\varphi, \theta)}(\mathbf{k}) Y_m^n(\mathbf{k}) d\Omega(\mathbf{k}), \quad (52)$$

where  $\Omega(\mathbf{k})$  is a surface element of a unit sphere  $\Omega$ . For a 3D isotropic scattering environment, we have  $f_{\mathbf{k}(\varphi,\theta)}(\mathbf{k}) = \frac{1}{4\pi}$  and thus (52) reduces to

$$\alpha_m^n = \frac{1}{4\pi} \int_{\Omega} Y_m^n(\mathbf{k}) d\Omega(\mathbf{k}). \quad (53)$$

Using the fact that

$$Y_m^n\left(\frac{\mathbf{n}_{k_s} - \mathbf{n}_{l_s}}{\|\mathbf{n}_{k_s} - \mathbf{n}_{l_s}\|}\right) = \frac{1}{\sqrt{4\pi}} \quad \text{if } n = m = 0, \quad (54)$$

and

$$\int_{\Omega} Y_m^n(\tilde{\mathbf{k}}) d\Omega(\tilde{\mathbf{k}}) = \begin{cases} \sqrt{4\pi} & \text{if } n = m = 0, \\ 0 & \text{otherwise,} \end{cases} \quad (55)$$

(51) can be rewritten as

$$[\mathbf{J}_s]_{k_s, l_s} = \delta_s^2 j_0(2\pi \|\mathbf{n}_{k_s} - \mathbf{n}_{l_s}\|), \quad (56)$$

which gives (1). Note that (1) conforms with [45]–[47] since  $j_0(c) = \frac{\sin c}{c}$ . In addition, (1) can be reduced to a 1D fluid antenna with 2D scattering environment by setting  $N_2^s = 1$  and  $\frac{0}{0} \triangleq 0$  and replacing  $j_0(\cdot)$  by  $J_0(\cdot)$  where  $J_0(\cdot)$  is the Bessel function of the first kind [9].

## APPENDIX II: GENERALIZATION TO OTHER SPATIAL CORRELATION MODELS

Without loss of generality, let us consider a 1D fluid antenna since a similar argument can be made for a 2D fluid antenna surface. To begin with, let us denote  $\mathbf{J}$  as the  $N \times N$  spatial correlation matrix. Suppose that  $W \gg 0$ , and the spatial correlation between the  $k$ -th and the  $l$ -th port is  $J_{k,l} = \delta^2 f(k, l, N)$  where the spatial correlation function  $f$  satisfies two conditions: i)  $\lim_{N \rightarrow \infty} f(k, k+1, N) = 1$  and ii) there are some  $\exists l \neq k$  such that  $f(k, l, N) \neq 1$ . The first condition implies that the  $(k+1)$ -th row/column of  $\mathbf{J}$  can be removed from  $\mathbf{J}$  since the  $(k+1)$ -th row/column of  $\mathbf{J}$  is always identical to the  $k$ -th row/column of  $\mathbf{J}$ . The second condition implies that there exist some  $l$ -th port whose  $l$ -th row/column must be retained in  $\mathbf{J}$  since its spatial correlation is distinct from the  $k$ -th port. If  $f$  satisfies these two conditions, then there must exist a minimal spacing  $c$  between the  $k$ -th and  $l$ -th ports such that their spatial correlation is distinct. Using the fact that  $W$  is finite, it is clear that there are at most  $\bar{N}$  non-identical ports since conditions (i) and (ii) hold. In particular,  $\bar{N}$  must be finite because  $W \geq \bar{N}c > 0$ . As a result,  $\mathbf{J}$  can be rewritten as a symmetric  $\bar{N} \times \bar{N}$  finite size matrix. Let us denote  $N'$  as the full rank of the symmetric  $\bar{N} \times \bar{N}$  matrix where  $N' \leq \bar{N}$ . Then, we can further reduce the symmetric  $\bar{N} \times \bar{N}$  matrix to a full rank symmetric  $N' \times N'$  submatrix  $\mathbf{J}_{\text{red}}$  by removing the  $(\bar{N} - N')$

dependent rows and columns. Consequently,  $\mathbf{J}$  can be represented by  $\mathbf{J}_{\text{red}}$  which is a full rank symmetric  $N' \times N'$  finite-size matrix.

## REFERENCES

- [1] F. Tariq *et al.*, “A speculative study on 6G,” *IEEE Wireless Commun.*, vol. 27, no. 4, pp. 118–125, Aug. 2020.
- [2] A. Shojaeifard *et al.*, “MIMO evolution beyond 5G through reconfigurable intelligent surfaces and fluid antenna systems,” *Proc. IEEE*, vol. 110, no. 9, pp. 1244–1265, 2022.
- [3] K. K. Wong, K. F. Tong, Y. Shen, Y. Chen, and Y. Zhang, “Bruce Lee-inspired fluid antenna system: Six research topics and the potentials for 6G,” *Frontiers in Commun. and Netw., section Wireless Commun.*, 3:853416, Mar. 2022.
- [4] Y. Huang, L. Xing, C. Song, S. Wang and F. Elhouni, “Liquid antennas: Past, present and future,” *IEEE Open J. Antennas & Propag.*, vol. 2, pp. 473–487, 2021.
- [5] A. Grau Besoli and F. De Flaviis, “A multifunctional reconfigurable pixeled antenna using MEMS technology on printed circuit board,” *IEEE Trans. Antennas & Propag.*, vol. 59, no. 12, pp. 4413–4424, Dec. 2011.
- [6] S. Song and R. D. Murch, “An efficient approach for optimizing frequency reconfigurable pixel antennas using genetic algorithms,” *IEEE Trans. Antennas & Propag.*, vol. 62, no. 2, pp. 609–620, Feb. 2014.
- [7] T. Ismail and M. Dawoud, “Null steering in phased arrays by controlling the elements positions,” *IEEE Trans. Antennas & Propag.*, vol. 39, no. 11, pp. 1561–1566, Nov. 1991.
- [8] S. Basbug, “Design and synthesis of antenna array with movable elements along semicircular paths,” *IEEE Antennas Wireless Propag. Lett.*, vol. 16, pp. 3059–3062, Oct. 2017.
- [9] K. K. Wong, A. Shojaeifard, K. F. Tong, and Y. Zhang, “Fluid antenna systems,” *IEEE Trans. Wireless Commun.*, vol. 20, no. 3, pp. 1950–1962, 2021.
- [10] K. K. Wong, A. Shojaeifard, K. F. Tong, and Y. Zhang, “Performance limits of fluid antenna systems,” *IEEE Commun. Lett.*, vol. 24, no. 11, pp. 2469–2472, 2020.
- [11] P. Mukherjee, C. Psomas and I. Krikidis, “On the level crossing rate of fluid antenna systems,” in *Proc. IEEE Int. Workshop Signal Process. Advances Wireless Commun. (SPAWC)*, 4-6 Jul. 2022, Oulu, Finland.
- [12] Z. Chai, K. K. Wong, K. F. Tong, Y. Chen, and Y. Zhang, “Port selection for fluid antenna systems,” *IEEE Commun. Lett.*, vol. 26, no. 5, pp. 1180–1184, May 2022.
- [13] L. Tlebaldiyeva, G. Naurzybayev, S. Arzykulov, A. Eltawil, and T. Tsiftsis, “Enhancing QoS through fluid antenna systems over correlated Nakagami- $m$  fading channels,” in *Proc. IEEE Wireless Commun. & Netw. Conf. (WCNC)*, pp. 78–83, 10-13 Apr. 2022, Austin, TX, USA.
- [14] L. Tlebaldiyeva, S. Arzykulov, K. M. Rabie, X. Li, and G. Naurzybayev, “Outage performance of fluid antenna system (FAS)-aided Terahertz communication networks,” in *Proc. IEEE Int. Conf. Commun. (ICC)*, 28 May-1 Jun. 2023, Rome, Italy.
- [15] M. Khammassi, A. Kammoun and M. -S. Alouini, “A new analytical approximation of the fluid antenna system channel,” *IEEE Trans. Wireless Commun.*, early access DOI:10.1109/TWC.2023.3266411.
- [16] W. K. New, K. K. Wong, H. Xu, K. F. Tong and C.-B. Chae, “Fluid antenna system: New insights on outage probability and diversity gain,” *IEEE Trans. Wireless Commun.*, early access, DOI:10.1109/TWC.2023.3276245.
- [17] C. Skouroumounis and I. Krikidis, “Fluid antenna with linear MMSE channel estimation for large-scale cellular networks,” *IEEE Trans. Commun.*, vol. 71, no. 2, pp. 1112–1125, Feb. 2023.
- [18] L. Zhu, W. Ma, B. Ning, and R. Zhang, “Movable-antenna enhanced multiuser communication via antenna position optimization,” [Online] arXiv preprint arXiv:2302.06978, 2023.

- [19] K. K. Wong, and K. F. Tong, "Fluid antenna multiple access," *IEEE Trans. Wireless Commun.*, vol. 21, no. 7, pp. 4801–4815, Jul. 2022.
- [20] N. Waqar, K. K. Wong, K. F. Tong, A. Sharples, and Y. Zhang, "Deep learning enabled slow fluid antenna multiple access," *IEEE Commun. Letters*, vol. 27, no. 3, pp. 861–865, Mar. 2023.
- [21] K. K. Wong, K. F. Tong, Y. Chen, and Y. Zhang, "Fast fluid antenna multiple access enabling massive connectivity," *IEEE Commun. Lett.*, vol. 27, no. 2, pp. 711–715, Feb. 2023.
- [22] H. Xu, K. K. Wong, W. K. New, and K. F. Tong, "On the outage probability for two-user fluid antenna multiple access," in *Proc. IEEE Int. Conf. Commun. (ICC)*, 28 May-1 Jun. 2023, Rome, Italy.
- [23] W. Ma, L. Zhu, and R. Zhang, "MIMO capacity characterization for movable antenna systems," [Online] arXiv preprint arXiv:2210.05396, 2022.
- [24] L. Zheng and D. Tse, "Diversity and multiplexing: A fundamental tradeoff in multiple-antenna channels," *IEEE Trans. Inform. Theory*, vol. 49, no. 5, pp. 1073–1096, May 2003.
- [25] K. K. Wong, K. F. Tong, and C. B. Chae, "Fluid antenna system-Part II: Research opportunities," *IEEE Commun. Lett.*, early access, DOI:10.1109/LCOMM.2023.3284318.
- [26] S. Sanayei and A. Nosratinia, "Antenna selection in MIMO systems," *IEEE Commun. Mag.*, vol. 42, no. 10, pp. 68–73, Oct. 2004.
- [27] A. Goldsmith, S. Jafar, N. Jindal, and S. Vishwanath, "Capacity limits of MIMO channels," *IEEE J. Select. Areas Commun.*, vol. 21, no. 5, pp. 684–702, Jun. 2003.
- [28] N. Iqbal, C. Schneider, and R. S. Thoma, "A fast and optimal deterministic algorithm for NP-Hard antenna selection problem," in *Proc. IEEE Int. Sym. Pers., Indoor, Mobile Radio Commun. (PIMRC)*, pp. 895–899, 30 Aug-2 Sep. 2015, Hong Kong, China.
- [29] A. Civril and M. Magdon-Ismail, "On selecting a maximum volume sub-matrix of a matrix and related problems," *Theoretical Comp. Sci.*, vol. 410, no. 47, pp. 4801–4811, 2009.
- [30] M. Gu and S. C. Eisenstat, "Efficient algorithms for computing a strong rank-revealing QR factorization," *SIAM J. Sci. Comp.*, vol. 17, no. 4, pp. 848–869, 1996.
- [31] W. Ford, *Numerical linear algebra with applications: Using MATLAB*, Academic Press, 2014.
- [32] N. Prasad and M. K. Varanasi, "Outage theorems for MIMO block-fading channels," *IEEE Trans. Inform. Theory*, vol. 52, no. 12, pp. 5284–5296, Dec. 2006.
- [33] Z. Wang and G. Giannakis, "A simple and general parameterization quantifying performance in fading channels," *IEEE Trans. Commun.*, vol. 51, no. 8, pp. 1389–1398, Aug. 2003.
- [34] L. Zhao, W. Mo, Y. Ma, and Z. Wang, "Diversity and multiplexing tradeoff in general fading channels," *IEEE Trans. Inform. Theory*, vol. 53, no. 4, pp. 1549–1557, Apr. 2007.
- [35] Y. Jiang and M. K. Varanasi, "The RF-chain limited MIMO system- part I: Optimum diversity-multiplexing tradeoff," *IEEE Trans. Wireless Commun.*, vol. 8, no. 10, pp. 5238–5247, Oct. 2009.
- [36] S.-G. Hwang, "Cauchy's interlace theorem for eigenvalues of Hermitian matrices," *The American Math. Monthly*, vol. 111, no. 2, pp. 157–159, 2004.
- [37] H. Moon, "Waterfilling power allocation at high SNR regimes," *IEEE Trans. Commun.*, vol. 59, no. 3, pp. 708–715, Mar. 2011.
- [38] A. Ghaderipoor, C. Tellambura, and A. Paulraj, "On the application of character expansions for MIMO capacity analysis," *IEEE Trans. Inform. Theory*, vol. 58, no. 5, pp. 2950–2962, May 2012.
- [39] S. H. Simon, A. L. Moustakas, and L. Marinelli, "Capacity and character expansions: Moment-generating function and



- other exact results for MIMO correlated channels,” *IEEE Trans. Inform. Theory*, vol. 52, no. 12, pp. 5336–5351, Dec. 2006.
- [40] R. G. Gallager, *Principles of digital communication*, Cambridge University Press Cambridge, UK, vol. 1, 2008.
- [41] L. Zheng and D. Tse, “Communication on the Grassmann manifold: A geometric approach to the noncoherent multiple-antenna channel,” *IEEE Trans. Inform. Theory*, vol. 48, no. 2, pp. 359–383, Feb. 2002.
- [42] P. C. Hansen, “The truncated SVD as a method for regularization,” *BIT Numerical Math.*, vol. 27, pp. 534–553, 1987.
- [43] E. Bjornson, J. Hoydis, L. Sanguinetti, *Massive MIMO networks: Spectral, energy, and hardware efficiency*, vol. 11. Now Foundations and Trends, 2017.
- [44] R. Mehrem, “The plane wave expansion, infinite integrals and identities involving spherical Bessel functions,” *Appl. Math. & Comp.*, vol. 217, no. 12, pp. 5360–5365, 2011.
- [45] R. K. Cook, R. Waterhouse, R. Berendt, S. Edelman, and M. Thompson Jr, “Measurement of correlation coefficients in reverberant sound fields,” *J. Acoustical Society of America*, vol. 27, no. 6, pp. 1072–1077, 1955.
- [46] R. W. Heath Jr and A. Lozano, *Foundations of MIMO communication*, Cambridge University Press, 2018.
- [47] E. Bjornson and L. Sanguinetti, “Rayleigh fading modeling and channel hardening for reconfigurable intelligent surfaces,” *IEEE Wireless Commun. Lett.*, vol. 10, no. 4, pp. 830–834, Apr. 2021.